OPTICAL AND STRUCTURAL PROPERTIES OF ZINC BASED NANOPARTICLES DEPEND ON TEMPERATURE AND MOLAR CONCENTRATION

by

ALFONSO JUAN HINOJOSA

Presented to the Faculty of the Graduate School of

The University of Texas at Arlington in Partial Fulfillment

of the Requirements

for the Degree of

MASTER OF SCIENCE IN PHYSICS

THE UNIVERSITY OF TEXAS AT ARLINGTON

December 2008

ACKNOWLEDGEMENTS

It is with heartfelt and infinite appreciation that I thank God for helping me to reach one more of my goals. I proceed to sincerely thank Dr. Chen, my advisor, not only for his great example of perseverance and fine leadership but also for his staunch support and understanding, and guidance. I also thank Dr. Weiss and Dr. Fry for their unforgettable lessons and examples as well as for their unconditional support and guidance.

Last but not least I thank my mother, Maria Teresa Perez-Hinojosa, and my father, Raul Hinojosa for their eternal love and constant support. I am also appreciative of both of my sisters Delia Josefina H. Mendez and Teresa Isabel H. Ramos for their love and support.

November 18, 2008

ABSTRACT

OPTICAL AND STRUCTURAL PROPERTIES OF ZINC BASED
NANOPARTICLES DEPEND ON TEMPERATURE
AND MOLAR CONCENTRATION

Alfonso Juan Hinojosa, M.S.

The University of Texas at Arlington, 2008

Supervising Professor: Dr. Wei Chen

Zinc based nanoparticles have great potential for use in radiation detection as well as uses in solid state lighting. In this thesis, we report the synthesis of ZnO: Eu3+ with the use of solid state diffusion at temperatures between 600 C and 700 C. We found that the emission of the nanoparticles depends particularly on the synthesis temperature as well as the molar concentration. The emission of the samples can be tuned to either the wavelengths of 495 nm and 611 nm. The formation of ZnO: Eu3+ has been identified with the use the Transmission Electron Microscope (TEM). The TEM showed that crystal fringes formed with a lattice constant of .50 nm. In addition, we conducted studies of ZnS: Co2+ and ZnS: Ag1+ which showed that the oxidation of the samples will change the luminescent properties of the samples. With the use of the X-Ray Diffraction Data (XRD), we showed that the diffraction peaks of the samples are characteristic peaks of either ZnO or ZnS depending on the cooking conditions. We use a straightforward approach of synthesizing the samples which have a major impact on developing sample which are tunable to different emission peaks.

TABLE OF CONTENTS

LIST OF ILLUSTRATIONS

CHAPTER 1

INTRODUCTION

1.1 Overview

Its applications in flat emission displays (FED's) and plasma display panels (PDP's) have recently brought attention from the scientific community to zinc oxide, (ZnO) an ideal candidate as a luminescent material [1,2,3,4]. Moreover, ZnO has many intrinsic properties which have led to innovations in the world of optoelectronic devices. Because of these intrinsic properties; it is used in research for biological uses. [4]

Solid state diffusion and different concentrations of europium (III) oxide doped into zinc oxide, as well as proper cooking conditions, will obtain a sharp red emission due to the energy transfer from the host lattice ZnO to the activator ions Eu^{3+}. Many researchers have declared that Eu^{3+}, one of the rare earth elements known for providing better luminescence because of its 4f intrashell transition, which gives a narrow peak luminescence, [5] doped into ZnO will produce only a weak emission of red light [5], while others have declared that the Eu^{3+} doped into ZnO will produce an intense red emission of light. The purpose of the current study is to investigate the conditions which are necessary for Eu^{3+} doped into ZnO to produce bright red luminescence [1, 2, 3, 4]. The investigation will also provide further evidence on the temperature dependence of Eu^{3+} doped into ZnO and the temperature at which Eu^{3+} doped onto ZnO transforms from red luminescence to green luminescence. This investigation gives a better understanding of how molar concentrations versus temperature dependence will change the physical characteristic of Eu^{3+} doped into ZnO and, therefore, change the luminescence the samples will emit. To effectively understand the physical mechanisms of Eu^{3+} doped onto ZnO, measurements must be taken to quantify the mechanisms of the phosphor.The most promising feature of ZnO is that it is

the most capable and chemically secure form of the oxide based phosphors. Furthermore, ZnO has a wide band gap energy of 3.37 eV and an exciton binding energy of 60 meV, which givethe ability to be doped with an activator ion that will change the phosphor luminescence.

To effectively understand the physical mechanisms of Eu^{3+} doped into ZnO, measurements must be taken to quantify the mechanisms of the phosphor. The instruments used to conduct these investigations will be Photoluminescence (PL), X-Ray Diffraction (XRD), and X-Ray Photoelectron Spectroscopy (XPS).

This investigation will also cover how ZnS: Co^{2+} and ZnS: Ag luminosity intensity, as well as how the position of the emission are directly related to the dopant ion, which is placed within the sample, and the conditions in which these samples are cooked. This investigation will also demonstrate how the increase in impurities will cause an optical quenching to take place within the sample for ZnS: Co^{2+}. The second thing that will be presented is how different conditions for ZnS: Ag will cause a shift in the emission peak and how it can be reversely engineered.

This thesis consists of four chapters. Chapter 1 introduces the history and the mechanism of scintillation, as well as the instruments used in the project. Chapter 2 presents analysis of the experimental data of zinc oxide doped with Eu^{3+}. Chapter 3 includes the discussion of the experimental results of zinc sulfide doped with silver chloride as well as the zinc sulfide doped with cobalt chloride. Chapter 4 contains the conclusion of the thesis and the analysis of the results.

1.2 History of Scintillation

In 1895, Wilhelm Röntgen discovered how to produce and emit x-rays; however, when Röntgen attempted to capture the images that x-rays would produce and transfer them onto photographic film, his efforts were fruitless because of the amount of time it took for the x-rays to

construct an image, particularly if the image was that of a human being because of the amount of damage the tissue would receive during the process. Therefore, to make this technology more efficient Röntgen turned to phosphors, which have the ability to release light after receiving a dose of ionizing radiation and consequently are able to release light that can be captured onto a photographic film and produce the image of the subject. The first phosphor to be used in x-ray detection was $CaWO_4$, which had a density of 6.6 gm/cm^3. [6] After this groundbreaking discovery was recognized, other researchers followed. For example, Ernest Rutherford used zinc sulfide (ZnS) to detect alpha particles being deflected off gold foil and William Crookes used ZnS to sense and count radioactivity [6] in his experiments with cathode ray tubes.

Another major contribution occurred in the 1940's when Robert Hofstadter developed a thallium-activated sodium iodide phosphor which contributed in the development of the Photomultiplier Tube (PMT), which allows for the user to be able to detect a single photon. Therefore, PMT's with their high gain, low noise and high frequency response [6] are able to adjust the intensity at which the photons are detected by a factor of 10^8 which will provide a better apparatus for detection. As a valuable result of this discovery, fields of medical imaging, astrophysics, and high energy physics were able to enhance the accuracy of their experimental results.

Another major progress for phosphors occurred in the 1950's with the development of glass scintillators, which were normally composed of lithium. Glass scintillators had a major advantage over typical scintillators because they were not affected by organic or inorganic materials, and they could function between wide temperature ranges. In addition, the evolution of alkali halide scintillators allowed for better radiation detectors since the presence of the alkali metal provided the scintillator with high stopping power for ionizing radiation, which proved for a more efficient phosphor. [10]

More recently, an emerging field has begun to take shape by decreasing the size at which matter is manipulated. This field, known as nanotechnology, will eventually change the scientific and engineering structural landscape because it allows for matter to be manipulated at a smaller scale. Nanotechnology was first envisioned in 1959 by famed physicist Dr. Richard Feynman in his speech given to the American Physical Society entitled “There’s Plenty of Room at the Bottom, An Invitation to a New Field of Physics”. Feynman aspired to one day have the ability to maneuver individual atoms in order to design components which would be able to operate under the nanoscale, which is defined as having the dimension of 10^{-9}m in all three spatial dimensions. These components themselves would then have the ability to be able to manufacture and construct components of equal size in order to perform many desirable functions. However, as the dimension of the governing matter decreases, different laws of physics become more prominent, such as quantum mechanics and statistical mechanics, which provide distinguishing features between macroscopic particles and nanoscaled particles. One such feature is the phenomenon governed by quantum mechanics known as nanoparticle luminescence, which is ruled by quantum size confinement. Quantum size confinement occurs when optoelectronic properties are changed by reducing the size of the nanoparticle thus bringing together holes and electrons at a distance close in size the exciton Bohr radius. Therefore, luminescence of nanoparticles depends on the size of the particle. Another distinguishing feature is the surface area to volume ratio between macroscopic particles and nanoparticles because it provides the altering mechanical, thermal and catalytic properties of materials.

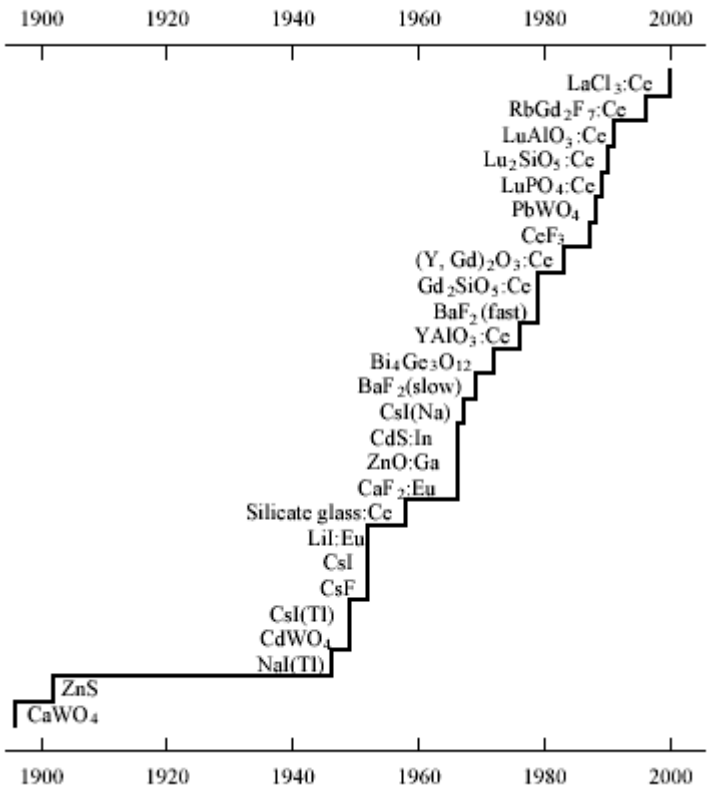

Fig. 1.1 Shows the history of the discovery of important inorganic materials

1.3 Evolution of Scintilators in Medical Imaging

Three major fields in physics, astrophysics, medical imaging, and high energy physics which depend heavily on the use of scintillators to be able to function and gather data. However, the field which is most beneficial to mankind is the field of medical imaging. It has been strongly dependent on photographic film, which captures images produced by scintillators. Another has been the development of digital capturing and process devices, which provide greater image resolution and ability to manipulate images.

When Röntgen took an image of his wife's hand with the use of x-rays in 1895, a wide door was opened to an enormous progression in the development of more sensitive scintillators which can now be used for medical imaging purposes. The first major advancement occurred in

the form of the scintillator used in the medical imaging devices. The discovery by Robert Hofstadter of NaI: TI in conjunction with the invention of the photomultiplier tube contributed immensely to the field of nuclear medical imaging noninvasive clinical examinations. However, because of the low density of NaI: TI (3.37g/cm^3), the spatial resolution was limited. The alternative was in the form of bismuth germanate (BGO), which had a density of 7.12 g/cm^3 and is now a part of a large fraction of the gamma ray medical imaging market. The BGO not only provides gamma ray imaging with good spatial resolution, but also has good radiation hardness, which can withstand 5x10^{4}Gy, and high scintillation efficiency.

The next breakthrough occurred in the form a innovative technique developed by the Japanese Fuji Corporation; it became known as Photo Stimulated Luminescence (PSL), a phenomenon that occurs when ionizing radiation strikes the storage phosphor and causes an electron to jump from the valence band to the conduction band. These free charge carriers become trapped in electron traps and hole traps. The traps are localized energy states within the phosphor, and are caused by impurities and lattice defects. There are two methods that can be used to release the stored energy within these states. The first is known as thermally stimulated luminescence, which uses heat as a form of energy to release the free charges which are within traps to recombine with trapped electrons or holes to release energy in the form of a photon. The other is photo stimulated luminescence, which strikes the irradiated phosphor with an incident photon which provides energy to allow the free charge carriers to recombine with the trapped hole and electrons, thus allowing a form of energy to be released in the form of a photon. This method has given to the advent of digital radiography which has several advantages over conventional film radiographic machines.

1.4 Physical Mechanism of Scintillation

The physical mechanism of scintillators occurs as ionizing radiation hits the scintillator and is divided into three stages. The first stage takes place when ionizing radiation strikes the

scintillator and produces inner shell holes. When ionizing radiation strikes the K shell, energetic primary electrons are formed in the conduction band. This is strongly based on the condition that the ionizing radiation has to be two to six times the energy of the band gap of the scintillator. The number of electrons and holes created by ionizing radiation is based on the following equation [7]

$N_{e\text{-}h} = E_{incident}/E_{e\text{-}h.}$

Following this event, secondary x-rays, which could hit other atoms, are produced and, in turn cause an F shell or L shell transition. Nonradiative processes then occur in the form of Auger electrons and create electrons in the conduction band and holes in the core and valence bands [8], which occur simultaneously with inelastic electron-electron scattering. This process takes place in the time domain of 10^{-15} to 10^{-12}s. [6]

The second stage occurs when hot electrons become less energetic than the ionization threshold energy. During this process, there can be two events which take place. The first is the production of phonons within the scintillator. The second process is a byproduct of phonons, which occur in the form of low kinetic energy electrons occurring below the conduction band as well as holes above the valence band. [14] After this occurrence, luminescent centers become excited by any of the following events between a time period of $<10^{-12}$ to $>10^{-8}$s: impact of hot electrons, electron-hole capture, hole-electron capture, or sensitizer-activator energy transfer.

The final stage takes place when the excited luminescent species return to the ground state in the form of a nonradiative process or by releasing the energy it has stored in the form of a photon.

1.5 Types of Scintillators

In nature there are three types of crystal materials that are known as conductors, insulators and semiconductors. There are two different types of semiconductors which exist in nature which have intrinsic and extrinsic properties. Intrinsic materials are semiconductors that

are known as activated scintillators, inherently possessing conductive properties caused by impurities or thermal properties. In an intrinsic semiconductor, the number of free charge carriers within the semiconductor is therefore established by the properties of the semiconductor instead of the amount of impurities. In addition, the number of excited electrons in an intrinsic semiconductor is equal to the number of holes; therefore, these types of semiconductors will exhibit luminescence core valence band transitions.

Extrinsic semiconductors are activated scintillators that are a part of the species which consists of a host lattice and an activator ion. The purpose of the activator ion is to shorten the band gap in order to change the luminescent properties of the semiconductor. [9] The activator ion known as a dopant will provide the semiconductor with holes or electron concentration which are known as acceptors or as donors, commonly known as p-type or n type semiconductors, respectively. The donor impurity atoms will have an excess of valence electrons in comparison to that of the host lattice in which it is being placed. Therefore, the donor atoms will provide valence electrons to the host lattice within the conduction band. The next type of activation ion is known as p type which will provide the host lattice with an excess of holes. These holes will lie below the Fermi energy level of the semiconductor that will give the scintillator an excess of holes within the valence band which will lie closer than the conduction band.

1.6 Preparation of Scintillators

The main objective in the preparation of the phosphors is being able to dissolve an activator ion, which contains impurities and is responsible for luminescence, into a crystal host lattice for the purpose of taking measurements and considering possible applications. [9] One begins by choosing high purity grade chemicals [9] and measuring these chemicals on an electronic scale to give an exact amount difference between the activator ions' weight and the host lattice's weight. These chemicals are then moved into Coors crucibles, high form, 15 ml, porcelain made by Sigma-Aldrich. The heating conditions in which these crucibles are placed in

the furnace differ only by the crucibles being enveloped in charcoal to prevent oxidation or being placed in air depending on the conditions of the experiment. Then the crucible which is in the Isotemp Muffle Furnace, made by Fisher Scientific, and can run between the temperatures of 25°C to 1100°C, can be cooked for any desirable time. During this time the process known as solid state diffusion takes place.

1.7 Experimental Setup

After the samples are done cooking in the furnace, they are taken out and placed into sample containers and properly identified. After this, physical measurements which include Photoluminescence, Electro-Paramagnetic Resonance, X-Ray Photo-Spectroscopy, Transmission Electron Microscope, and Lifetime, must be taken.

1.7.1 Photoluminescence

The Shimadzu spectrofluorophotometer system RF-5301 PC was used to take photoluminescence measurements. The system is based on the principle known as fluorescence. It states that certain materials which absorb electromagnetic energy will push the electrons of the material into a higher energy state $S_0 + h\nu_{ex} \rightarrow S_1$ and re-emit energy in the form of lower energy photons emitted $S_1 \rightarrow S_0 + h\nu_{em}$ known as a Stokes Shift. There are two types of emission which occur: fluorescence and phosphorescence. Fluorescence is the emission which occurs spontaneously upon excitation and ceases to emit after the source has been removed. It has a decay lifetime of picoseconds, nanoseconds, and microseconds. The phosphorescence is emission that persists after the exciting source is removed. It has a decay lifetime of milliseconds, seconds, and hours. The light source which provides the electromagnetic energy is a 150 Watt Xenon lamp. Another principle which is applied to photoluminescence is known as quantum efficiency. It is measured using the equation $Q = n_e / n_e + n_f$ where n_e , defined as the frequency of light emission and n_f is defined as the frequency of non-radiation emission of

your sample which is useful in determining the effectiveness of your sample.

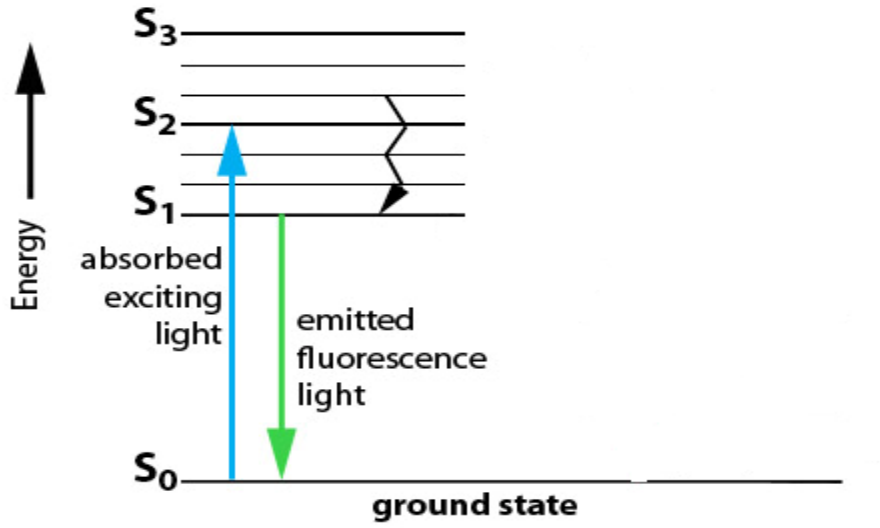

Fig. 1.2 Exhibits a schematic diagram of the process of fluorescence.

1.7.2 Transmission Electron Microscope

One must begin by examining the history of the TEM which began in 1924 after Louis de Broglie predicted that all matter will possess a duality of both particle and wavelike properties. Using this principle, in addition to the principles which were formed using light microscopes, a beam of electrons created by thermionic emission is accelerated through a potential V which then makes impact with the sample to create an image as the electrons interact and travel through the specimen. The next and final stage occurs as an image is captured by an objective lens and monitor. Therefore, in order to gain a better perspective on the sample which is being used, one must be able to study the crystalline structures of the samples to determine the outcome of one's experiment. The TEM being used is provided by Oklahoma State University at the Microscopy Lab.

1.7.3 X-Ray Photoelectron Spectroscopy

X-Ray Photoelectron Spectroscopy (XPS) is a technique which is primarily based on the photoelectric effect, which quantitatively gives the chemical composition, empirical formula, and the chemical and electronic states of the samples. The process begins by creating an ultra high vacuum within the chamber which houses the sample and continues by etching the sample with an ion beam to do away with surface contaminants. Then it follows by first irradiating the ample with either aluminum or magnesium x-rays which then hit the sample and cause photoelectrons to be released. This which will allow for the kinetic energy and number of electrons to be detected and measured empirically statement of Ebinding = Ephoton – Ekinetic –Φ. This measurement will give two quantities which are the amount of electrons which were released as well as the binding energy of the elements which will also give details of the electron configuration. The XPS which was sued for this was taken at the University of Texas at Arlington in the Chemistry Department.

1.7.4 X-Ray Diffraction

X-Ray Diffraction (XRD) is a physical measurement which can determine the composition of materials by determining the arrangement of atoms within the crystal structure by the scattering of electrongs with the crystal. XRD utilizes the fact that the crystal structure has a periodic structure which is formed by lattice vectors or basis vectors. Once a crystalline sample is prepared, it is placed on a goniometer where the sample is then irradiated, using monochromatic x-rays which then cause the atoms within the crystal to scatter electrons. These electrons then cause a reflection or what is better known as the diffraction pattern. The sample is then rotated by varying the degrees at which the x-rays bombard the sample. This allows for more reciprocal space to be observed, and detected by using photographic film or an image sensor.

CHAPTER 2

LUMINESCENT AND STURUCTUAL PROPERTIES OF ZINC OXIDE DOPED WITH EU^{3+}

2.1 Introduction and Basic Properties

One of the oxide phosphors which have been studied extensively is the phosphor zinc oxide. Throughout its history zinc oxide has found its way into many applications which include medical, biosensor, optoelectronic and radiation detection in space research. Recently it has gained attention because of possible applications to flat emission displays and plasma display panels. It has also been considered a prime candidate for nanodevice material because of its potential as a very attractive host lattice for doping several luminescence centers and shows versatile applications. [4] Zinc oxide is a wide band gap semiconductor with a lattice constant of 4.58 Å which has a band gap energy of 3.37 eV, and a binding energy of 60 meV, this giving it the advantage of efficient emission processes can carry on in ZnO at room temperature and higher. [10] ZnO exhibits an emission peak at around 550 nm which can be attributed to the superposition of green and red emission due to the self activated centers and strongly ionized oxygen vacancies. [11]

2.1.1 Semiconductor Properties of Zinc Oxide

The valence band of ZnO and the lowest conduction band both occur at the Γ point k=0 which implies that the crystal structure of zinc oxide has a direct band gap. [6] In addition, the large energy gap of zinc oxide provides an ideal situation during which rare earth elements could produce, and provide polychromatic displays. Rare earth elements which are used as activator

ions are known for providing better luminescence because of their 4f intrashell transition which gives a narrow peak luminescence [12]. As stated by S.A.M Lima, et. al, the luminescent properties of trivalent rare earth (RE^{3+}) depend on their host. [2] In addition, activator ions which are doped into host lattices will provide the lattices with impurities which will change the luminous properties of the host lattice.

2.1.2 Optical Properties of Zinc Oxide

The main component which is responsible for semiconductor luminescent properties is the exciton. An exciton is defined as an electron and a hole which are present in an insulator or a semiconductor and are both attracted together by Coulomb force. An exciton can be either a free exciton or a bound exciton. In an intrinsic semiconductor, optical transitions take place between electrons which are located within the conduction band and holes which are located within the valence band. This also includes effects produced by excitons, acting under the influence of Coulomb interactions. In an extrinsic semiconductor, optical transitions take place because of impurities, point defects or dopants, which are inserted into the host lattice and usually generate electronic states in the band gap. [11] Because of this, the optical assimilation and the emission route depend heavily on these factors.

Within this research, ZnO: Eu3+ is widely observed to emit only a green luminescence except under appropriate conditions, which show a red luminescence occurring. The source of the green luminescence has been controversial for many decades as many have attributed this to be due to copper impurities. However, recently the most widely accepted argument is that the green luminescence exists because of the oxygen vacancies which are present within the samples.

2.1.3 Structural Properties of Zinc Oxide

The band gap which is present within zinc oxide provides an ideal situation in which rare earth elements are placed to create impurities to change the optical absorption and emission process. The lattice constant of zinc oxide has been determined to be 4.5 Å and has four atoms per unit cell.

2.2 Current Investigation

The facility to be able to observe 4f electron emission by ZnO:Eu^{3+} under UV light still remains uncertain. The first study to be reported was done by Kouyate D. in 1991 in the Journal of Luminescence in which case luminescence by RE^{3+} elements remained extremely elusive [5]. Additional studies have been performed which have demonstrated only weak red emission had been observed from phosphors containing zinc oxide doped with euporium (III) chloride or europium (III) oxide [3]. Others have demonstrated a strong red luminescence being produced by phosphors containing zinc oxide doped with euporium (III) chloride or europium (III) oxide [1]. One of these studies included a paper written by Zhang, Lin Li in 2005. In the Chinese Physics Letters Lin Listated that a strong red luminescence appeared under UV excitation can be observed. The chemicals used in this paper were zinc oxide, europium (III) oxide and lithium nitrate, which were mixed in a beaker with ethanol and baked at a temperature of 900°C [12]. The results demonstrated that an energy transfer from ZnO host to Eu^{3+} ions can be observed. [12] Therefore, this matter merits further studies to investigate the physical and chemical mechanisms of Eu3+ doped into zinc oxide.

This work will show that by using the method of solid state diffusion and by considering different concentrations of europium (III) oxide doped into zinc oxide one will obtain a sharp red emission due to the energy from the host lattice ZnO to the activator ions Eu^{3+}. The investigation will also provide further evidence on the temperature dependence of $Eu3^{+}$ doped into ZnO and the temperature at which Eu^{3+} doped onto ZnO will transform from a red luminescence to green

luminescence. This study will give a better understanding of how molar concentrations versus temperature dependence will change the physical characteristic of Eu^{3+} doped onto ZnO and, therefore, change the luminescence the samples will emit. To effectively understand the physical mechanisms of Eu^{3+} doped onto ZnO, measurements were to quantify the mechanisms of the phosphor.

2.3 Preparation of Samples

The samples were prepared by first measuring zinc oxide and europium (III) oxide with the use of an electronic scale. The Eu^{3+} concentrations in zinc oxide varied within the realm of 7% to 16%. The samples were then mixed together with the use of a mortar and a pestle to grind the chemicals until a homogenous paste was developed. The sample was then placed into a Coors crucible, high form, 15 ml, porcelain made by Sigma-Aldrich which was either placed under charcoal to prevent oxidation or was left in the atmosphere of air. Then the crucible was then moved into the Isotemp Muffle Furnace which was used to cook the sample ranging between the temperatures of 600°C and 700°C. The samples were then allowed to cool, taken out from the furnace, placed into sample holders, and labeled properly.

2.4 Methods of Characterizing Samples

To effectively understand the physical mechanisms of Eu^{3+} doped into ZnO, measurements must be taken to quantify the mechanisms of the scintillator. The instruments which were used to conduct these investigations were Photoluminescence (PL),Tunneling Electron Microscope (TEM), X-Ray Photoelectron Spectroscopy (XPS) and Electro Paramagnetic Resonance (EPR).

2.5 Transmission Electron Microscope Data

The Transmission Electron Microscope operated by Oklahoma State University Microscopy Lab developed the following images which show the average particle size and the crystal structure size.

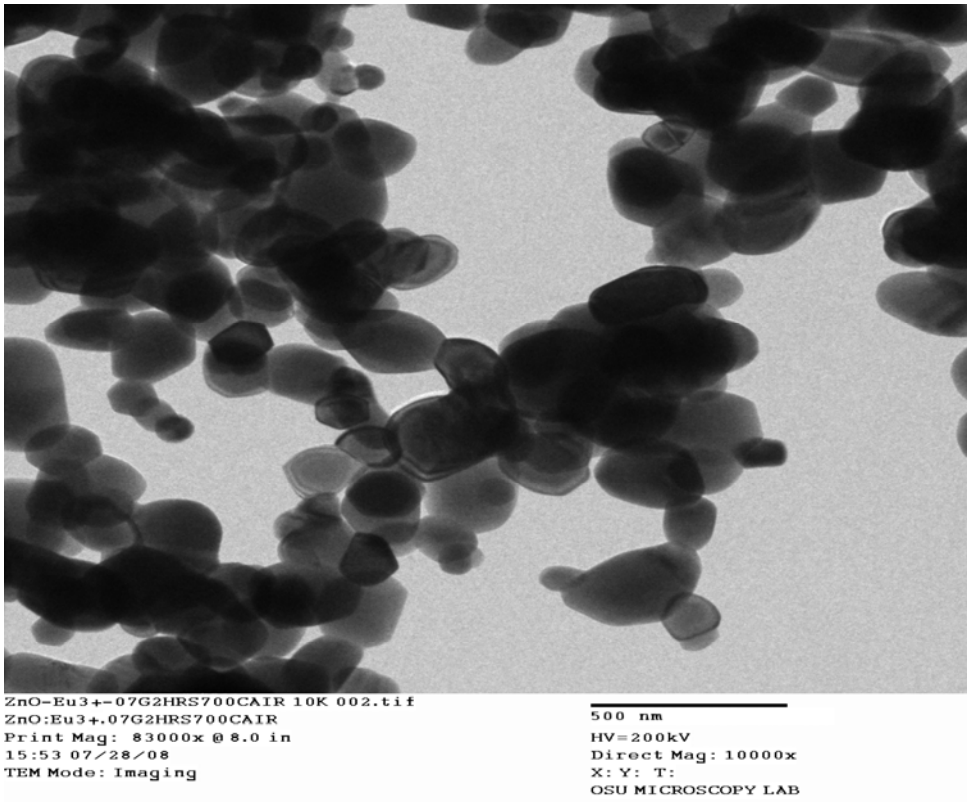

Fig. 2.1. TEM Data showing elliptically shaped particles formed of ZnO: Eu^{3+} .07 g 2 hrs 700C Air

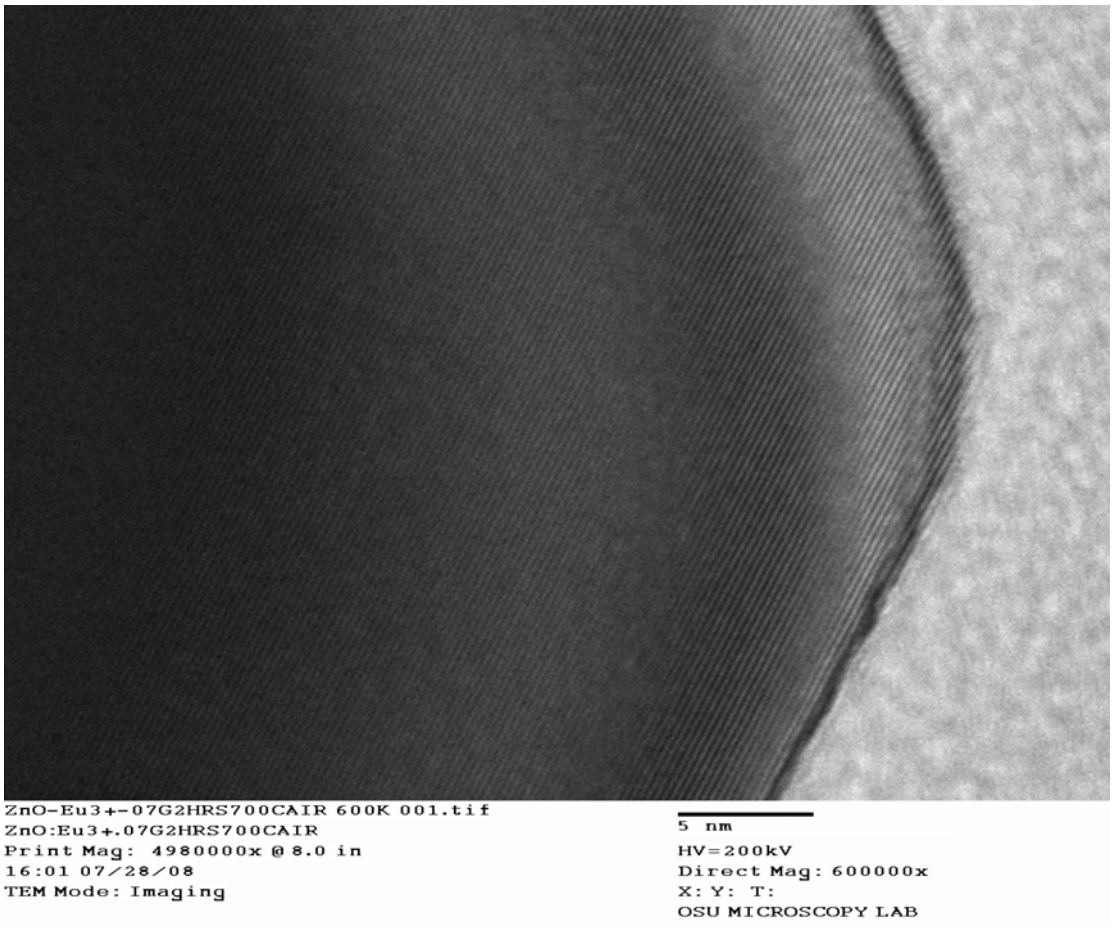

Fig 2.2 TEM Data showing lattice fringes created by the formation of ZnO: $Eu3^{+}$ .07 g 2 hrs 700C Air

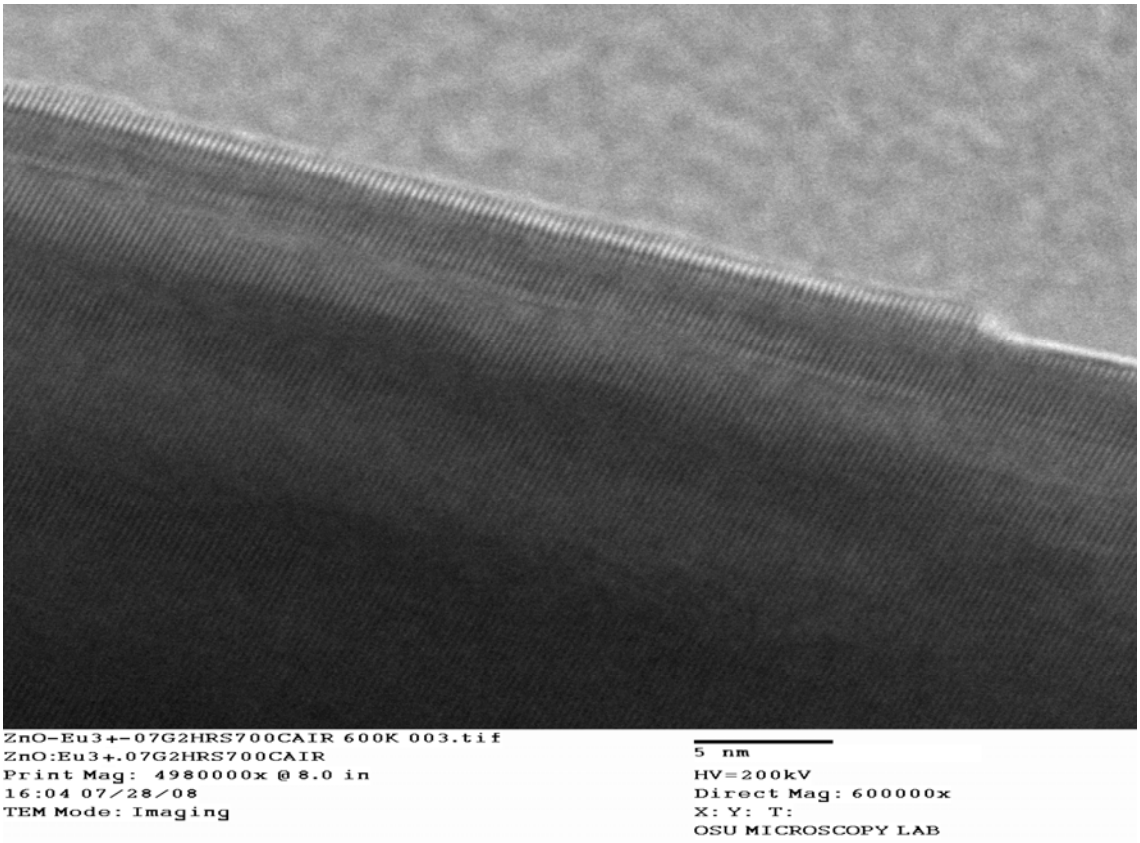

Fig. 2.3 TEM Data showing lattice fringes created by the formation of

ZnO: Eu^{3+} .07 g 2 hrs 700 C Air

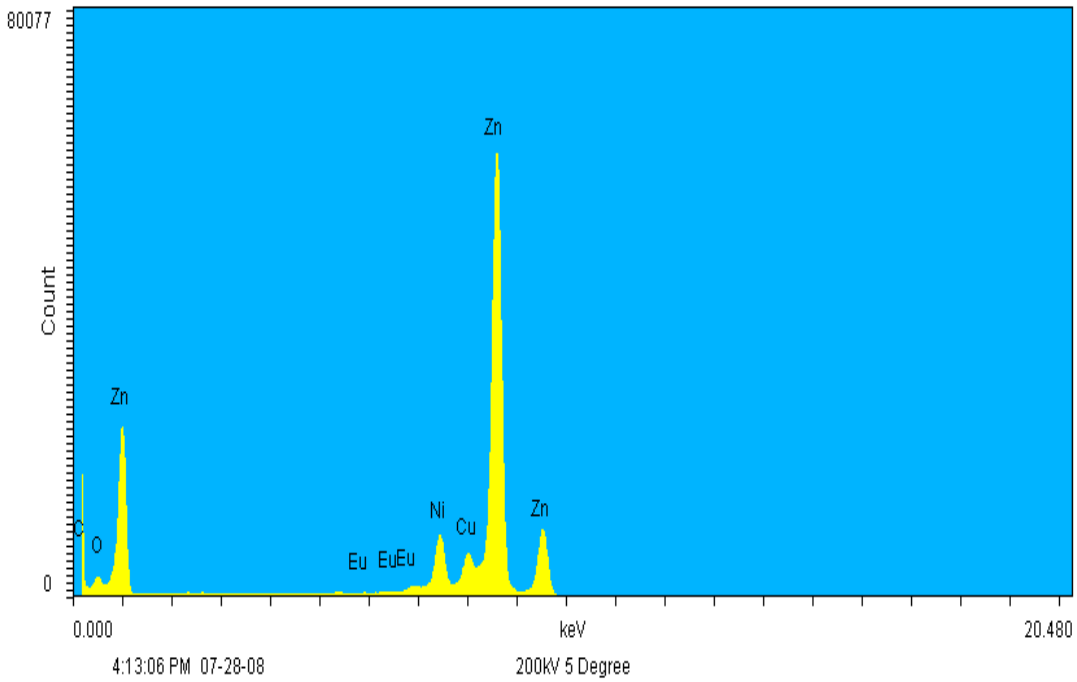

Identification result: Spectrum 1

C	0.206 keV
O	0.510 keV
Zn	1.001 keV
Eu	5.851 keV
Eu	6.460 keV
Eu	6.830 keV
Ni	7.470 keV
Cu	8.039 keV
Zn	8.670 keV
Zn	9.569 keV

Quant result: Spectrum 1

Fig. 2.4 EDS Data showing spectral data of the chemical composition of ZnO: Eu^{3+} .07 g 2hrs

Elements:	WT%	AT%	K_A	K_F	K_Z	Intensity	P/bkg
O K	10.06	31.37	0.132	1.002	1.081	39.24	5.1
ZnL	79.51	60.67	0.905	1	0.989	457.855	48.4
EuL	0	0	1.371	1.471	0.955	0	0
ZnK	10.43	7.96	1.054	1	0.99	1930.602	64.3

Fig. 2.5 EDS Data showing chemical composition of ZnO: Eu^{3+} .07 g 2 hrs

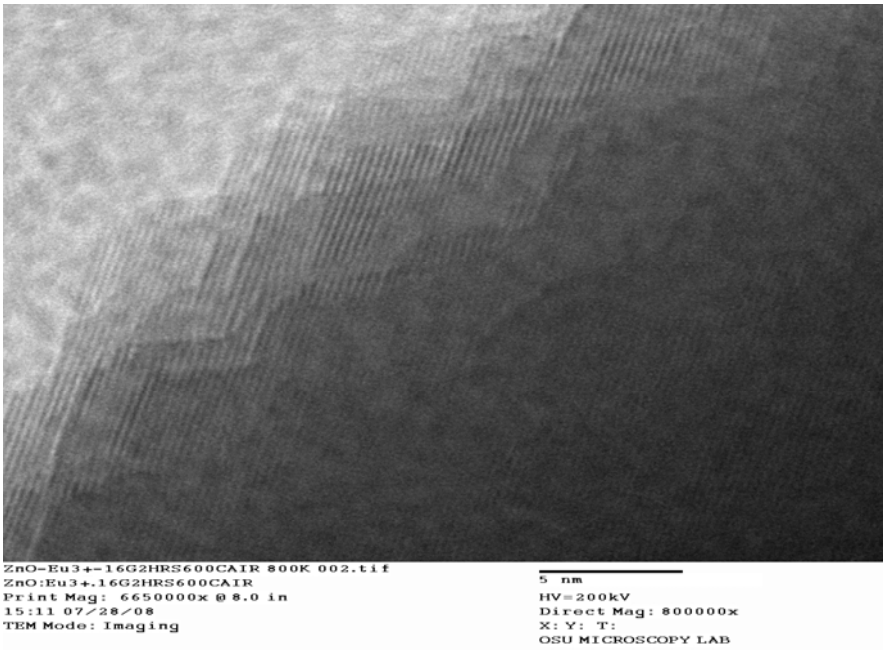

Fig. 2.6 TEM Data of lattice fringes formed by ZnO: Eu^{3+} .16g 2 hrs air 600C

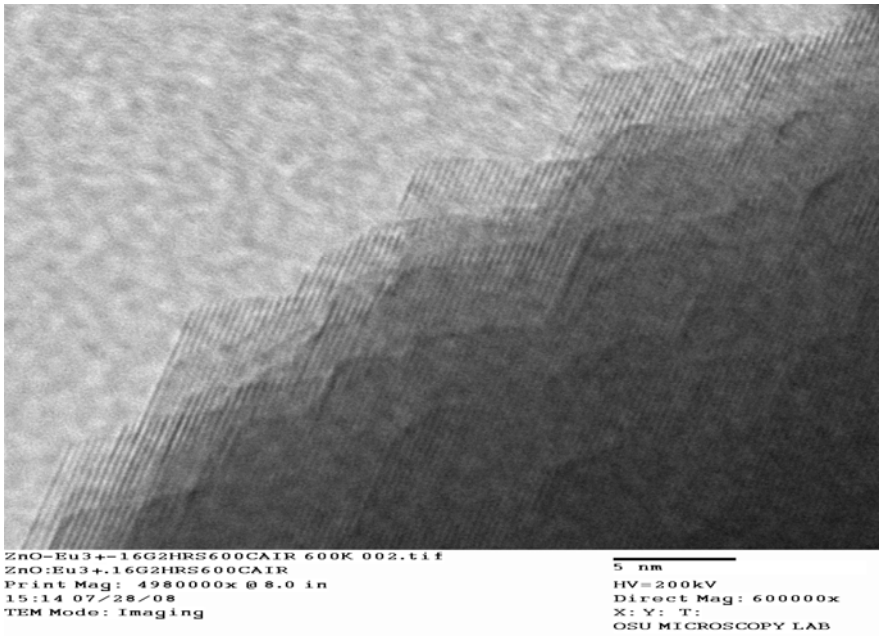

Fig. 2.7 TEM Data of lattice fringes formed by ZnO: Eu^{3+} .16g 2 hrs air 600C

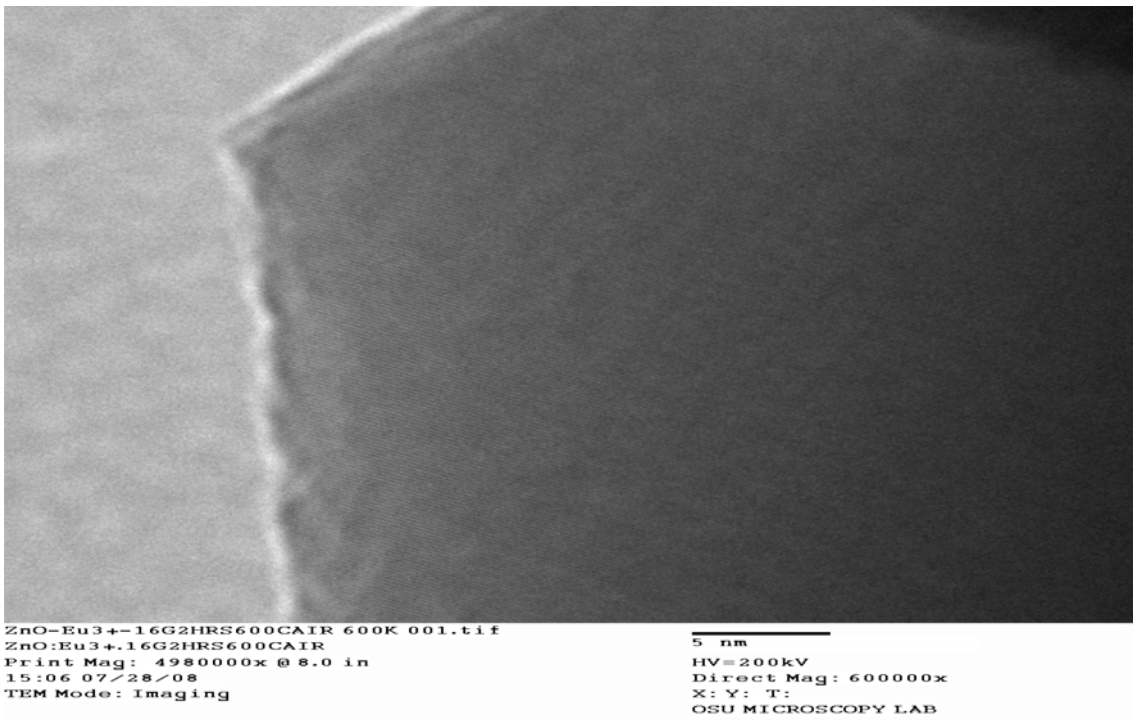

Fig. 2.8 TEM Data of lattice fringes formed by ZnO:Eu^{3+} .16g 2 hrs air 600C

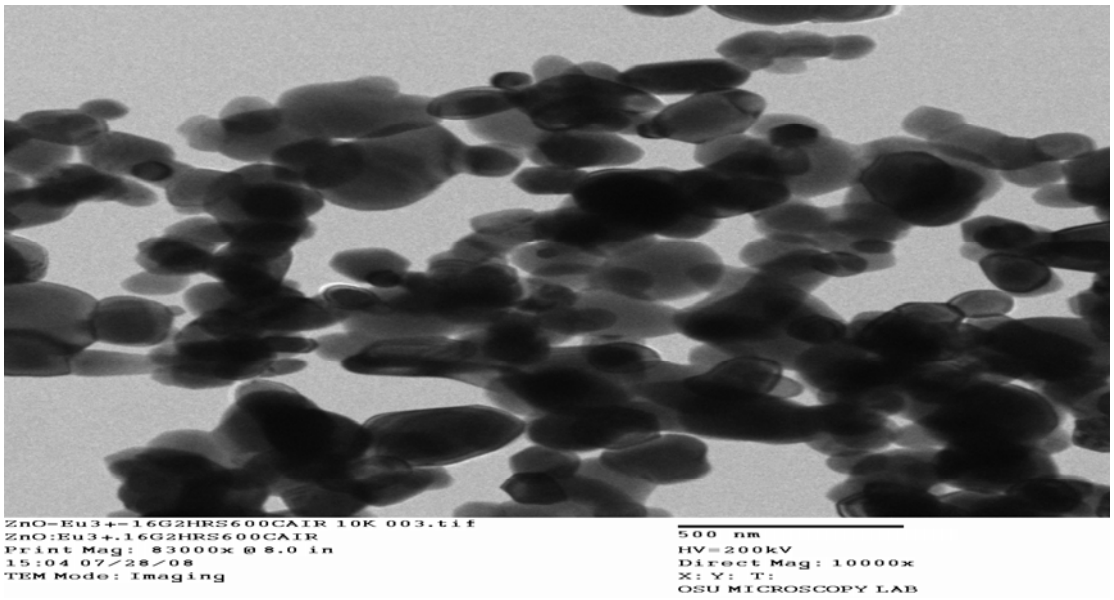

Fig. 2.9 TEM Data showing elliptically shaped particles formed by

ZnO: Eu^{3+} .16g 2 hrs air 600C

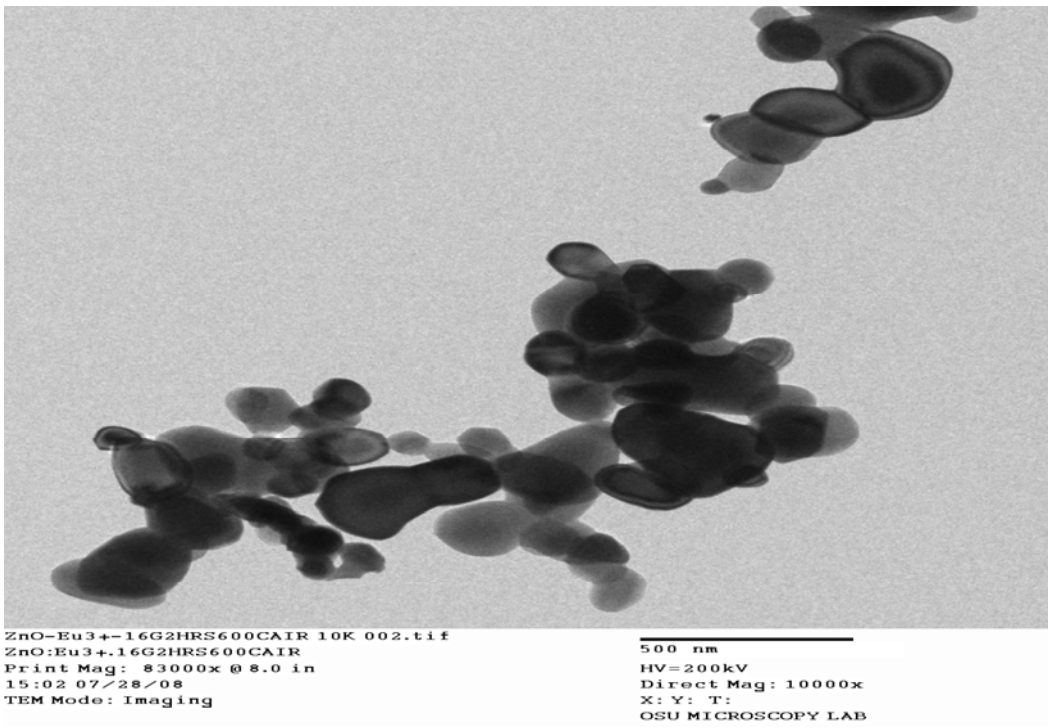

Fig. 2.10 TEM Data showing elliptically shaped particles formed by

ZnO: Eu^{3+} .16g 2 hrs air 600C

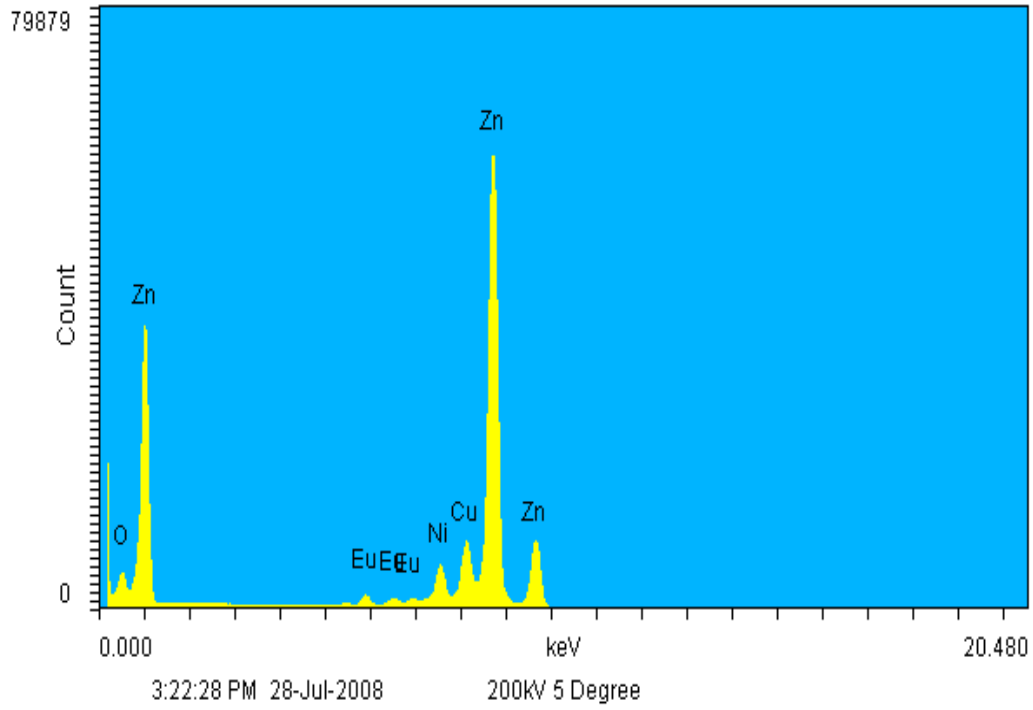

Identification result: Spectrum 2

O	0.510 keV
Zn	1.001 keV
Eu	5.851 keV
Eu	6.460 keV
Eu	6.830 keV
Ni	7.470 keV
Cu	8.039 keV
Zn	8.670 keV
Zn	9.569 keV

Quant result: Spectrum 2

Fig. 2.11 EDS Data showing the spectral showing spectral data of the chemical composition of ZnO: Eu^{3+} .16 g 2hrs air

Elements:	WT%	AT%	K_A	K_F	K_Z	Intensity	P/bkg
O K	11.37	34.42	0.134	1.002	1.079	58.493	5.6
ZnL	81.73	60.58	0.893	1	0.988	606.689	47.2
EuL	0.27	0.09	1.381	1.46	0.954	21.119	0.9
ZnK	6.63	4.91	1.044	1	0.988	1589.472	91.4

Fig. 2.12 EDS Data of ZnO: Eu^{3+} .16g 2 hrs air

The TEM images in Figs. 2.1, 2.8, 2.9 demonstrate that elliptically shaped particles of Eu^{3+} doped into zinc oxide which were synthesized using the solid state diffusion method can be observed. The TEM images in Figs. 2.2, 2.3, 2.5, 2.6, 2.7 shows a crystalline structure of Eu^{3+} doped on zinc oxide which were formed with the use of solid state diffusion. In addition, with the use of the length scale on the images, the crystal lattice constant is determined to be .5nm which coincides with the theoretical lattice constant of .45nm. Furthermore, the average particle size which was obtained and can be determined from the images is within the size realm of 300 nm. However, the study found that there is a difference between the two samples of .07g and .16g respectively. The sample which contains .07 g does not have any Eu^{3+} which is detectable and emits green luminescence. On the other hand, the sample which contains .16g does have Eu^{3+} which is present and emits a strong red luminescence.

Evidently, during the preparation of sample .07g which utilized solid state diffusion, the Eu^{3+} must have diffused during the process.

2.6 XPS Data for ZnO: Eu^{3+}

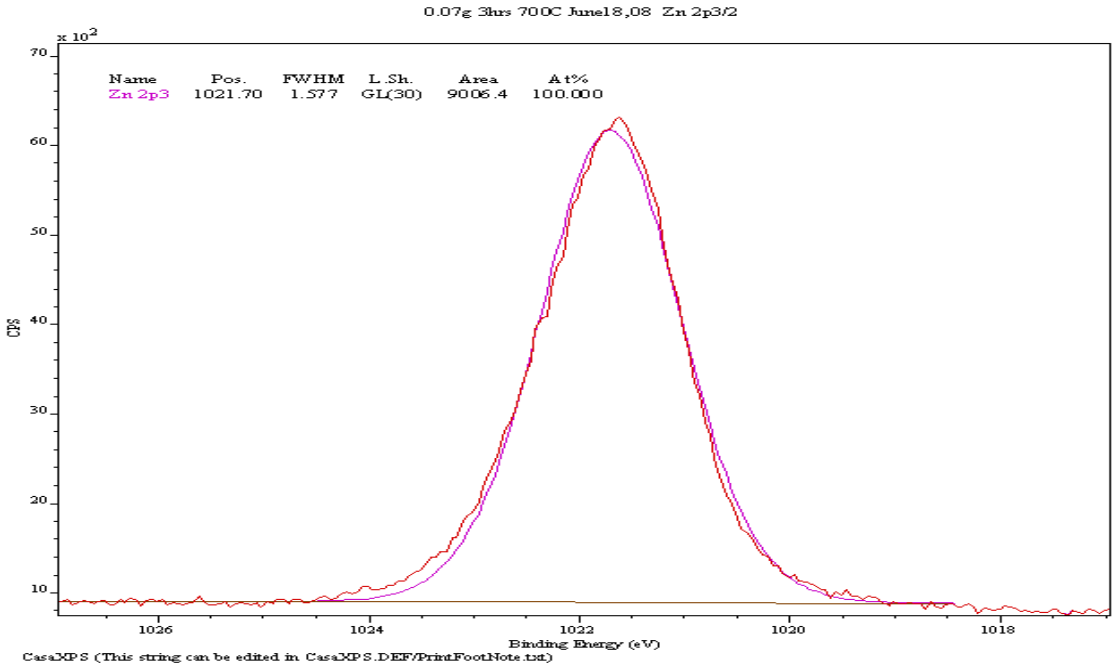

Fig. 2.13 XPS Data of ZnO: $Eu3^{+}$ .07g 3 hrs 700C showing the surface element of Zn 2p3

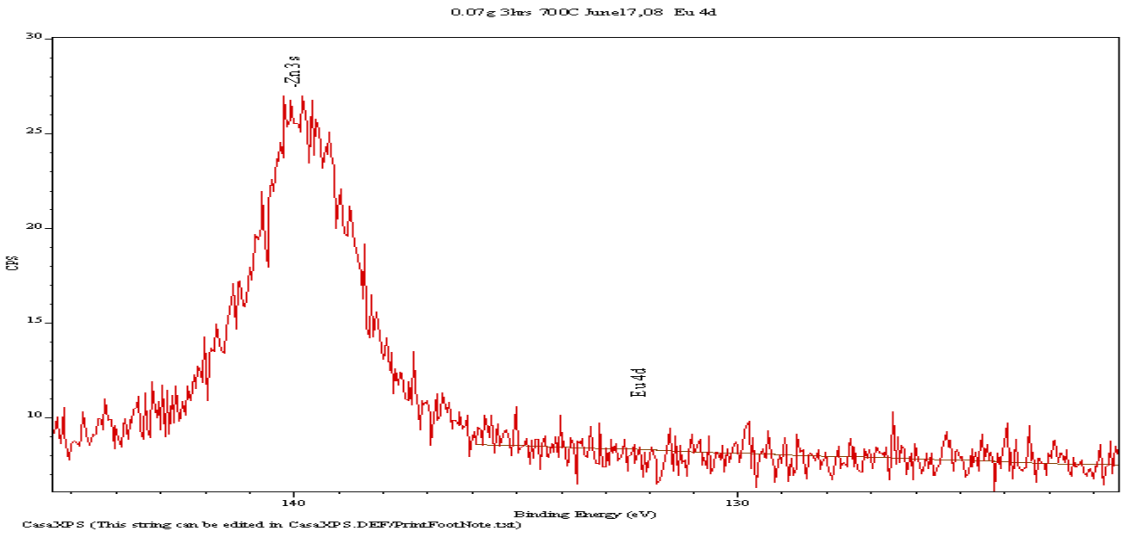

Fig. 2.14 XPS Data of ZnO: Eu^{3+} .07g 3 hrs 700C showing the surface element of Zn 3s

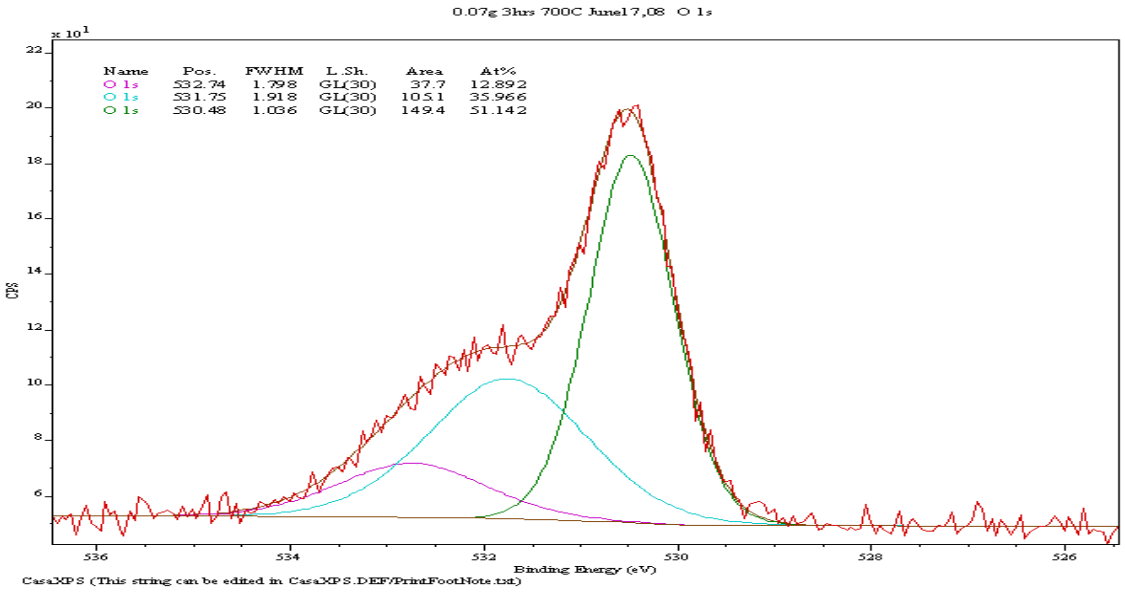

Fig. 2.15 XPS Data of ZnO: Eu^{3+} .07g 3 hrs 700C showing the surface element of O 1s

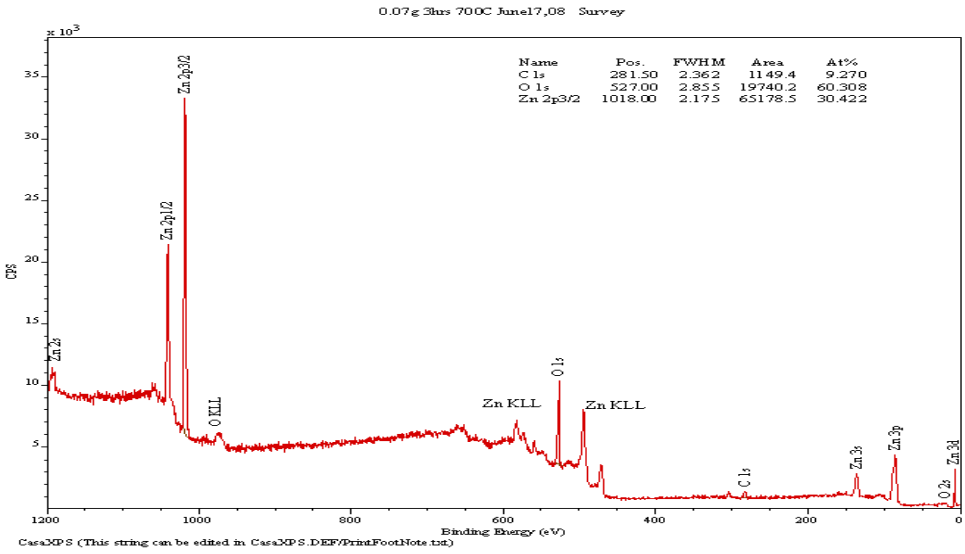

Fig. 2.16 XPS Data of ZnO: Eu^{3+} .07g 3 hrs 700C showing the wide spectra of all surface elements

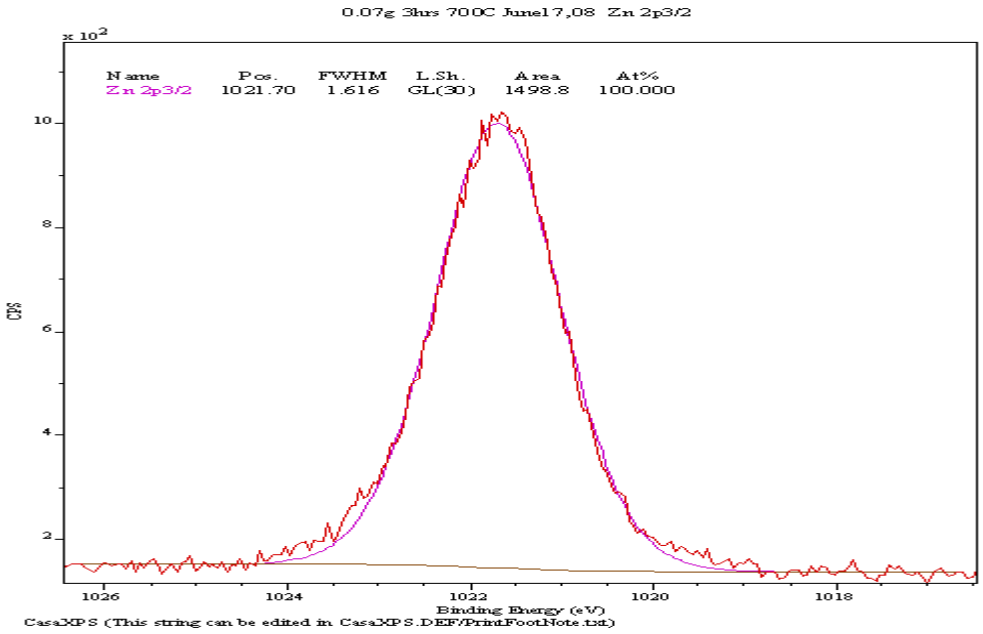

Fig. 2.17 XPS Data of ZnO:Eu^{3+} .07g 3 hrs 700C showing the surface element of Zn 2p3/2

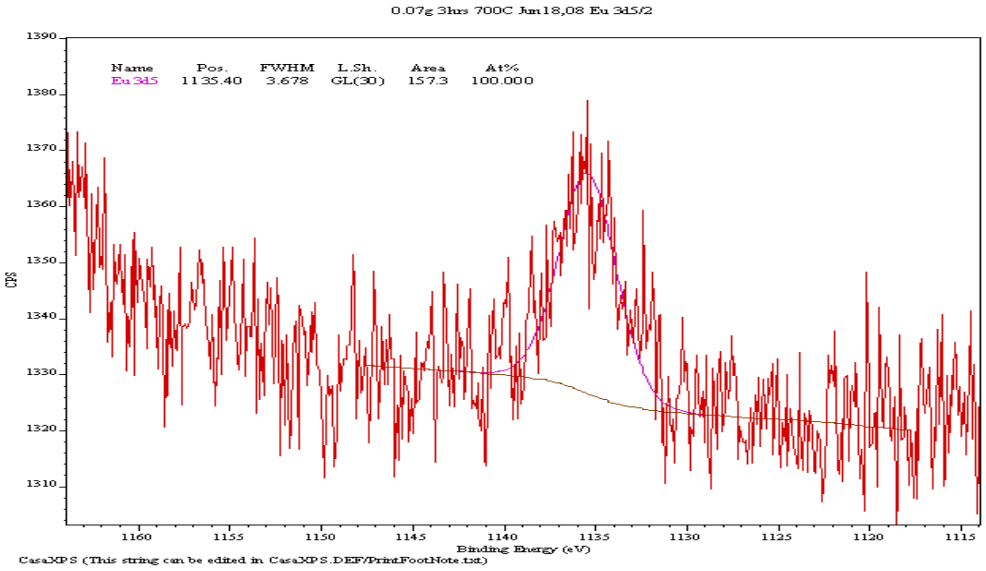

Fig. 2.18 XPS Data of ZnO: Eu^{3+} .07g 3 hrs 700C showing the surface element of Eu 3d5

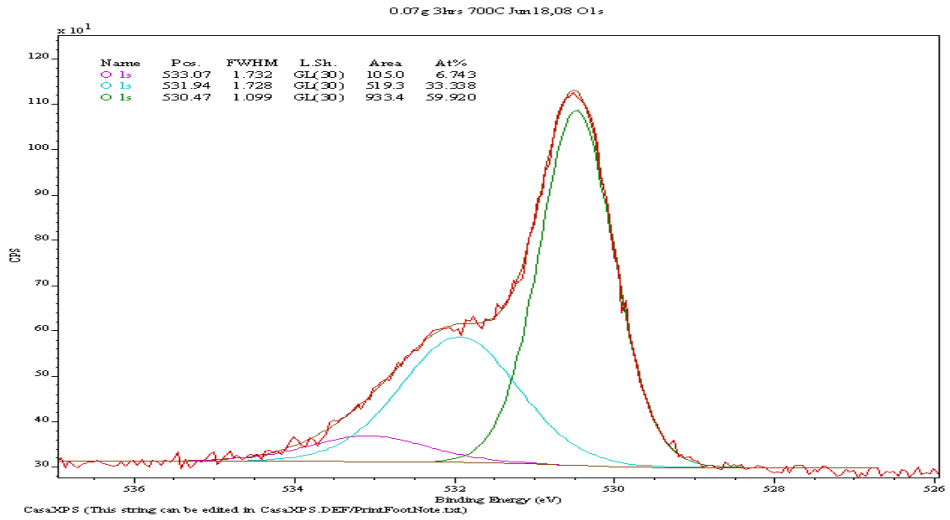

Fig. 2.19 XPS Data of ZnO: $Eu3^{+}$ .07g 3 hrs 700C showing the surface element of O 1s

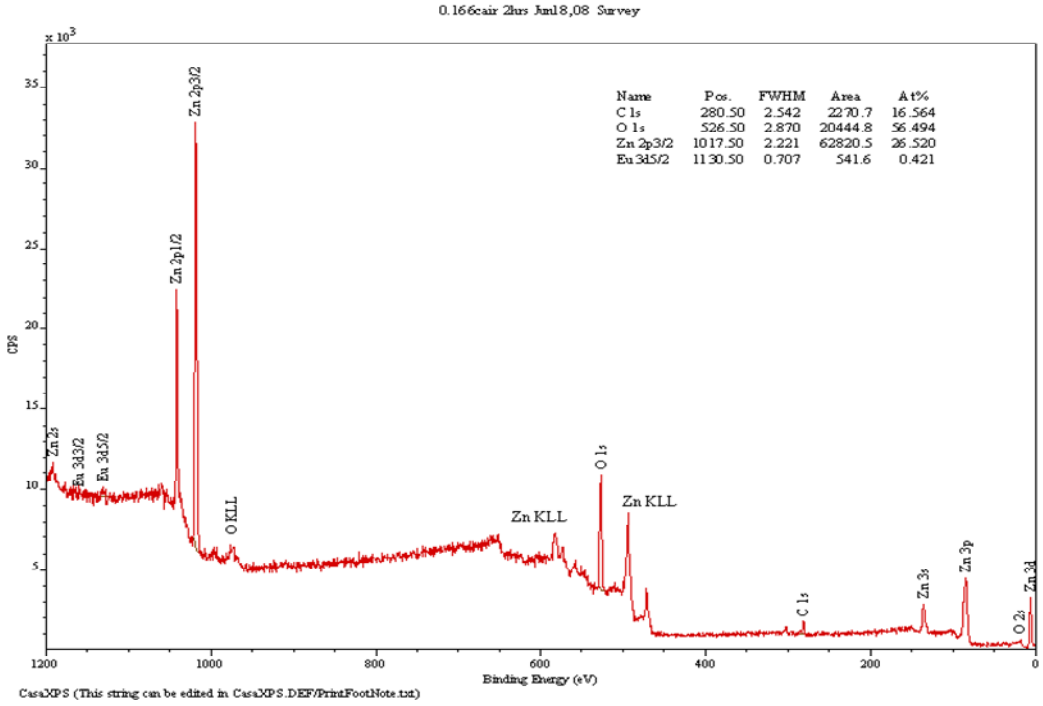

Fig. 2.20 XPS Data of ZnO: Eu^{3+} .07g 3 hrs 700C showing the wide spectra of all surface elements

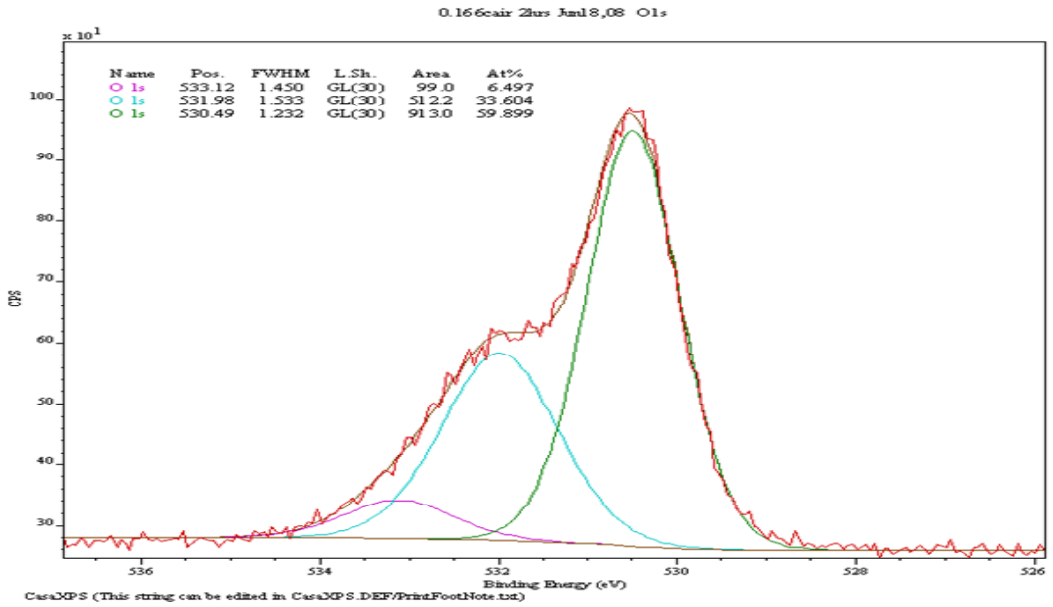

Fig. 2.21 XPS Data of ZnO:Eu^{3+} .16g 2 hrs 600C showing the surface element O 1s

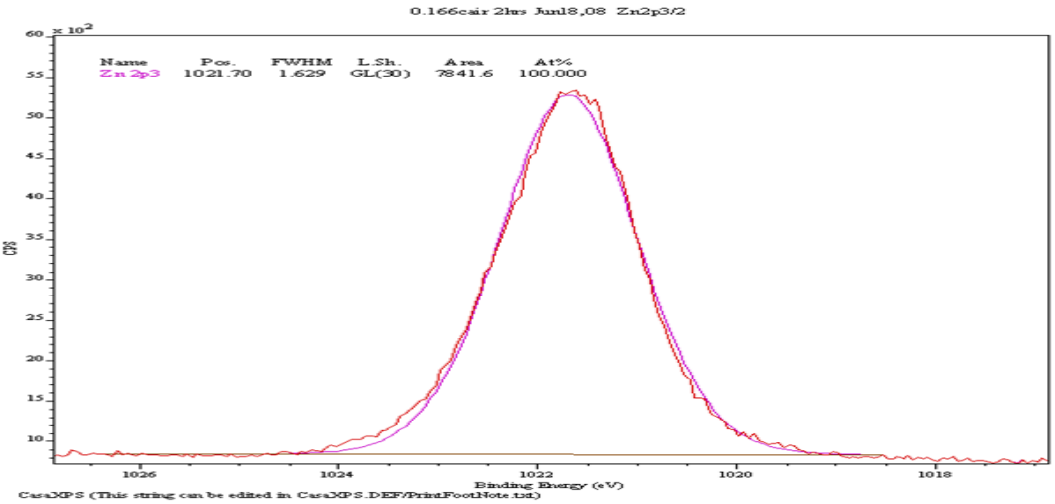

Fig. 2.22 XPS Data of ZnO:Eu^{3+} .16g 2 hrs 600C showing the surface element Zn 2p3

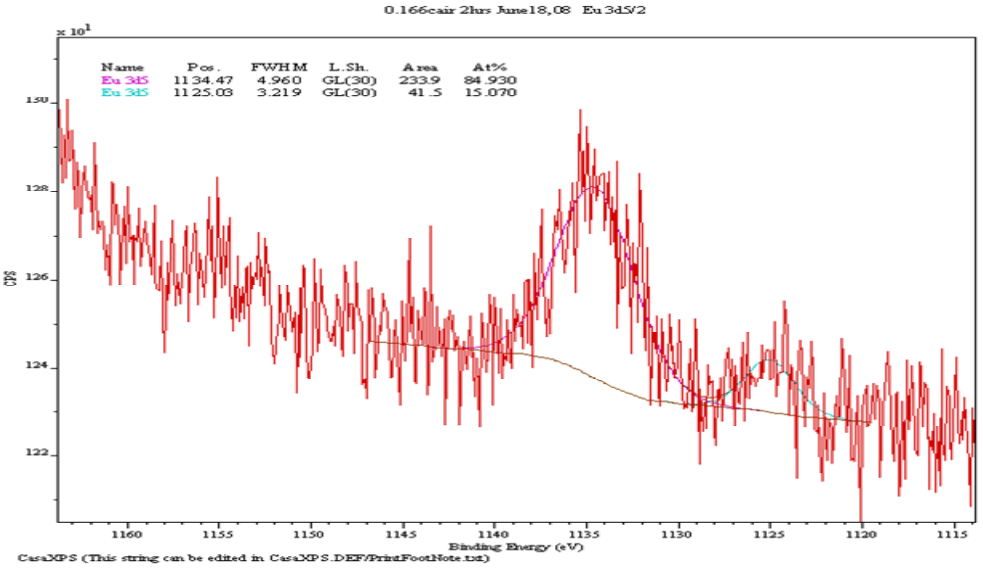

Fig. 2.23 XPS Data of ZnO:Eu^{3+} .16g 2 hrs 600C showing the surface element Eu 3d5

In figures 2.11 and 2.20, it is shown that the surface analysis reveals the chemical state is the same for both samples of Zn 2p3. In figures 2.17 and 2.19, it can be seen that the surface analysis reveals the chemical state is the same for both samples showing the electronic configuration of O 1s. In figures 2.16 and 2.21, it is shown that the electronic configurations for both samples are the same of Eu 3d5. In figures 2.14 and 2.18, it is shown that the wide spectra shows the same surface composition of the electronic configuration of chemicals including carbon which must have been picked up during the preparation of the samples.

2.7 Photoluminescence Data for ZnO: Eu^{3+}

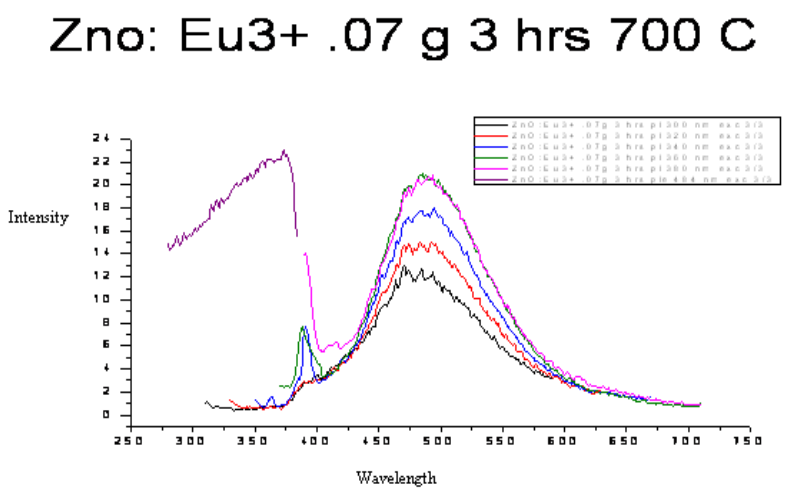

Fig 2.24 PL Data of ZnO: Eu^{3+} .07 g 3 hrs 700 C showing both the excitation and emission spectra

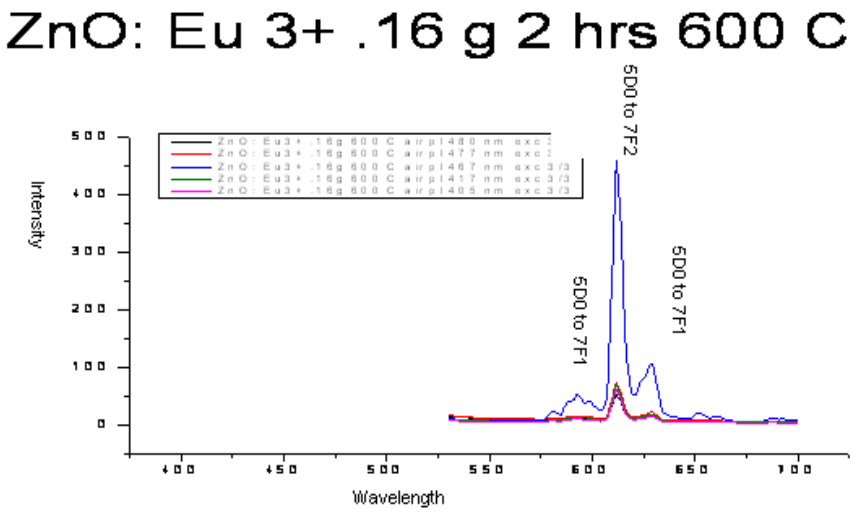

Fig. 2.25 PL Data of ZnO: Eu^{3+} .16 g 600 C showing both the excitation and emission spectra

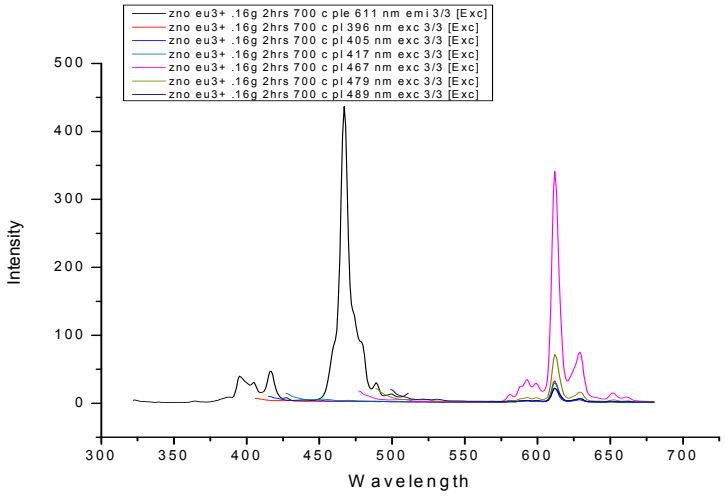

Fig. 2.26 PL Data of ZnO: Eu^{3+} .16 g 700 C showing both the excitation and emission spectra

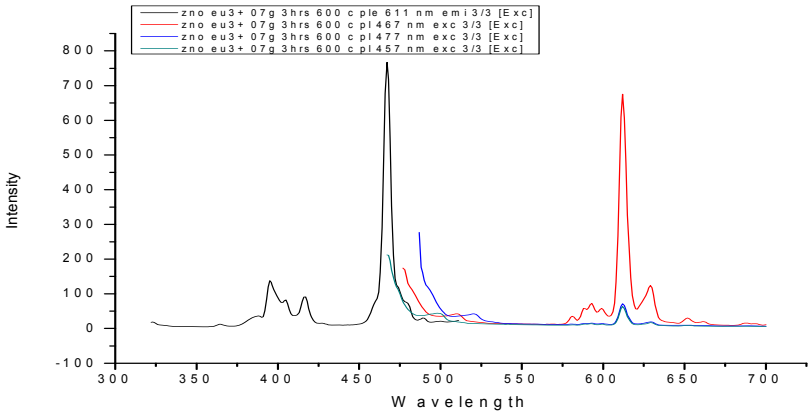

Fig. 2.27 PL Data of ZnO: Eu^{3+} .07g 600 C showing both the excitation and emission spectra

In figure 2.25, the PL spectra for ZnO: Eu^{3+} .07 g cooked for 2 hrs at 700 C shows the typical green luminescence peak centered around 494 nm which is done by ZnO and not Eu^{3+}. This is shown to be intrinsic defects of the ZnO matrix [4] and to the band to band exciatation [1]. These findings have been controversial for many decades, and many have attributed this to be due to copper impurities. However, recently the most widely accepted argument is that the green luminescence exists because of the oxygen vacancies, which are present within the samples. [2, 4] In addition, the graph illustrates the excitation spectrum which is shown to be centered on the 360 nm range which also shows that the most efficient excitation wavelength is between 360 nm and 380 nm.

Using past literature as a reference, figures 2.26, 2.27, 2.28 shows the PL spectra for ZnO: Eu^{3+} .16 g cooked for 2 hrs at 600 C, ZnO: Eu^{3+} .16g cooked for 2 hrs at 600 C, and ZnO: Eu^{3+} .07 g cooked for 2 hrs at 700 C, respectively, cooked for exhibits a central luminescence peak centered around 615 nm which is done by lowest excited states [4] of Eu^{3+} $^5D_0$ to ^7F_J transitions. Based on the spectral analysis, it is concluded that there are three major peaks which correspond to the $^5D_0$ to ^7F_J these are seen at 590 nm, 610 nm and 625 nm, which are related to the $^5D_0$ to $^7F_1$, $^5D_0$ to $^7F_2$ and $^5D_0$ to $^7F_3$ transitions. [4] The largest emission peak is centered at 615 nm, which was caused by 467 nm excitation wavelength.

2.8 Conclusion

ZnO: Eu3+ was synthesized by using the method of solid state diffusion. The Transmission Electron Microscope (TEM) clearly shows the crystal fringes which were formed which showed the lattice constant to be .50 nm which is in close agreement to the theoretical lattice constant of Zinc Oxide of .45nm. The X-Ray Photoelectron Spectroscopy (XPS) shows no difference in the surface composition of the samples. The samples have a difference in emission peak by showing that the .07 g has an emission peak around 494 nm which is primarily a green luminescence. As opposed to the other sample of .16g which has three major emission peaks

three major peaks which correspond to the $^5D_0$ to ^7F_J these are seen at 590 nm, 610 nm and 625 nm, which are related to the $^5D_0$ to $^7F_{1,}$ $^5D_0$ to $^7F_2$ and $^5D_0$ to $^7F_3$ transitions.

CHAPTER 3

LUMINESCENT AND STRUCTURAL PROPERTIES OF ZINC SULFIDE DOPED WITH Co^{2+} AND Ag^{1+}

3.1 Basic Properties

The first scintillator to be used by Ernest Rutherford for radiation detection was zinc sulfide. Rutherford who used this as a way of converting ionizing radiation into visible light which would be efficient for photographic film to study alpha particle scattering [6]. Since then the number of applications have grown to include uses in cathode ray tubes, which can emit light when excited by electrons. It also is used in glow in the dark products and infrared optical materials, which have applications in the fields of astronomy and medical physics. Recently, the compound zinc sulfide has been thought of as having further applications in the field of flat emission displays and plasma display panels [13, 14]. The compound zinc sulfide can be doped as an n-type semiconductor or as a p-type semiconductor. Zinc sulfide is found in nature as two basic shapes one which is hexagonal, and the other is the more stable cubic form. Both forms have a wide band gap energy; the cubic has a 3.54 eV and the hexagonal has a 3.91 eV band gap energy. The compound zinc sulfide exhibits an emission peak around 450 nm.

3.1.1 Semiconducting Properties

Zinc sulfide is a direct band semiconductor within the family of II-VI semiconductor family, which means that the valence band and the conduction band occur when the momentum k=0. The direct band gap transition gives the ideal situation where energy released from band to band transition is primarily in the form of electromagnetic radiation. In addition, the zinc sulfide

wideband gap makes it the best candidate for a blue light emitter. In order to manipulate the intensity of the luminescence by the host lattice, an activator ion must be added. By adding the activator, both the intensity of the luminescence and the emission peak of the semiconductor will change. Therefore, in this paper Silver Chloride, AgCl, and Cobalt (II) Chloride, $CoCl_2$ $6H_2O$ were added to the host lattice of Zinc Sulfide, ZnS. Adding these dopant ions will dramatically change the luminescent properties of Zinc Sulfide [13, 14].

3.1.2 Optical Properties

As stated in the previous chapter, the main component which is responsible for semiconductor luminescent properties is the exciton. An exciton is defined as an electron and a hole which are present in an insulator or a semiconductor, and are both attracted together by Coulomb force. An exciton can be either a free exciton or a bound exciton. In an intrinsic semiconductor, optical transitions take place between electrons which are located within the conduction band and holes which are located within the valence band. This also includes effects produced by excitons, acting under the influence of Coulomb interactions. In an extrinsic semiconductor, optical transitions take place because of impurities, point defects or dopants, which are inserted into the host lattice and usually generate electronic states in the band gap.[8] Because of this, the optical assimilation and the emission route depend heavily on these factors.

3.1.3 Structural Properties of ZnS

Zinc sulfide has two different structures, one cubical and the other hexagonal. These two different structures both have different lattice constants which are 5.420 Å for the cubic structure and a = 3.82 Å and c = 6.26 Å for the hexagonal structure. In addition to the structures, Zinc Sulfide also has a wide band gap energy which allows for dopant ions to influence the emission intensity as well the emission peaks.

3.2 Current Investigation

The recent advancement in flat emission displays as well as plasma display panels has increased the need for further study in zinc sulfide materials due to their efficient fluorescent abilities. Studies have demonstrated that zinc sulfide has been shown to have a dependency on dopant ions to increase luminescent efficiency and properties. In this study, solid state diffusion was used to synthesize the following nanoparticles of ZnS: AgCl and ZnS: $CoCl_2$ $6H_2O$ to see how different cooking conditions can change the luminescent properties. This study also demonstrated how an increase in amount of impurities in ZnS: $CoCl_2$ $6H_2O$ has a quenching effect on the luminescence of the fluorescent material. In addition, the oxidation of the sample ZnS: $CoCl_2$ $6H_2O$ will occur depending on whether the crucible in which the sample was cooked under was covered by charcoal or under the atmosphere of air. The second sample of ZnS : AgCl showed how impurities at a certain point also affect the efficiency of the luminescent material. In addition, it has been discovered that the emission peak of the sample can be reversed engineered, depending on the cooking conditions of the sample. For example, the ZnS: Ag^{1+} cooked under charcoal and ZnS: Ag^{1+} cooked under air had its luminescence changed by once again cooking them in different conditions. To make a point, have the one cooked in air now cooked under charcoal and the one cooked under charcoal now cooked in air. The interchange will be able to change the position peaks of the samples.

This research demonstrated that the ZnS: Co^{2+} and ZnS: Ag^{1+} luminosity intensity, as well as the position of the emission are directly related to the dopant ion which is placed within the sample. It also showed, in the sample for ZnS: Co^{2+}, that increase in impurities will cause an optical quenching to take place. The second thing that was illustrated demonstrated how different conditions for ZnS: Ag^{1+} will cause a shift in the emission peak and how this can be reversed engineered.

3.3 Preparation of the ZnS : AgCl and ZnS : $CoCl_2$ 6 H_2O

The samples were prepared by first measuring Zinc Sulfide and Cobalt (II) Chloride 6 H_2O with the use of an electronic scale. The Co^{2+} concentrations in Zinc Sulfide varied with the realm of 1% to 2%. The samples were then mixed together with the use of a mortar and a pestle to grind the chemicals until a homogenous paste was developed. The sample was then placed into a Coors crucible, high form, 15 ml, porcelain made by Sigma-Aldrich which was either placed under charcoal to oxidation or was left in the atmosphere of air. Then the crucible was moved into the Isotemp Muffle Furnace, which was used to cook the sample at the temperature of 700°C. The samples were then allowed to cool, taken out from the furnace, placed into sample holders, and labeled properly.

The next sets of samples were prepared by first measuring zinc sulfide and silver chloride with the use of an electronic scale. The Ag^{1+} concentrations in zinc sulfide varied within the realm of 2%, 5%, and 7%. The samples were then mixed together with the use of a mortar and a pestle to grind the chemicals until a homogenous paste was developed. The sample was then placed into a Coors crucible, high form, 15 ml, porcelain made by Sigma-Aldrich, which was either placed under charcoal to oxidation or was left in the atmosphere of air. Then the crucible was moved into the Isotemp Muffle Furnace, which was used to cook the sample at the temperature of 700°C. The samples were then allowed to cool and were taken out from the furnace, placed into sample holders, and labeled properly.

3.4 Methods of Characterizing Samples

To effectively understand the physical mechanisms of Co^{2+} and Ag^{1+} doped onto ZnS, measurements were taken to quantify the mechanisms of the scintillator. The instruments used to conduct these investigations were Photoluminescence (PL),Tunneling Electron Microscope (TEM), X-Ray Photoelectron Spectroscopy (XPS) and Lifetime measurements.

3.5 Photoluminescence Measurements of ZnS: CoCl2 6 H2O

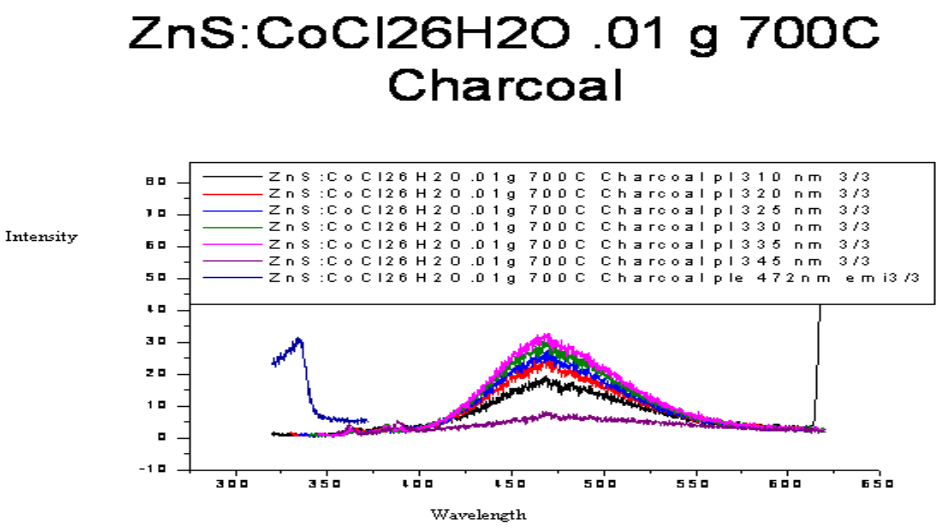

Fig. 3.1 PL Data of ZnS: $CoCl_2$ $6H_20$ .01 g 700 C Charcoal showing both the exciation and emission spectra

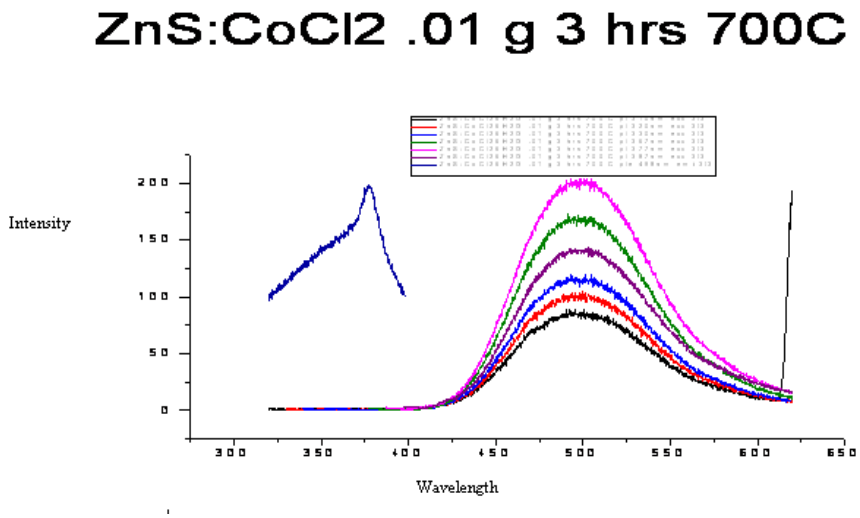

Fig. 3.2 PL Data of ZnS: $CoCl_2$ $6H_20$ .01 g 700 C showing both the excitation and emission spectra

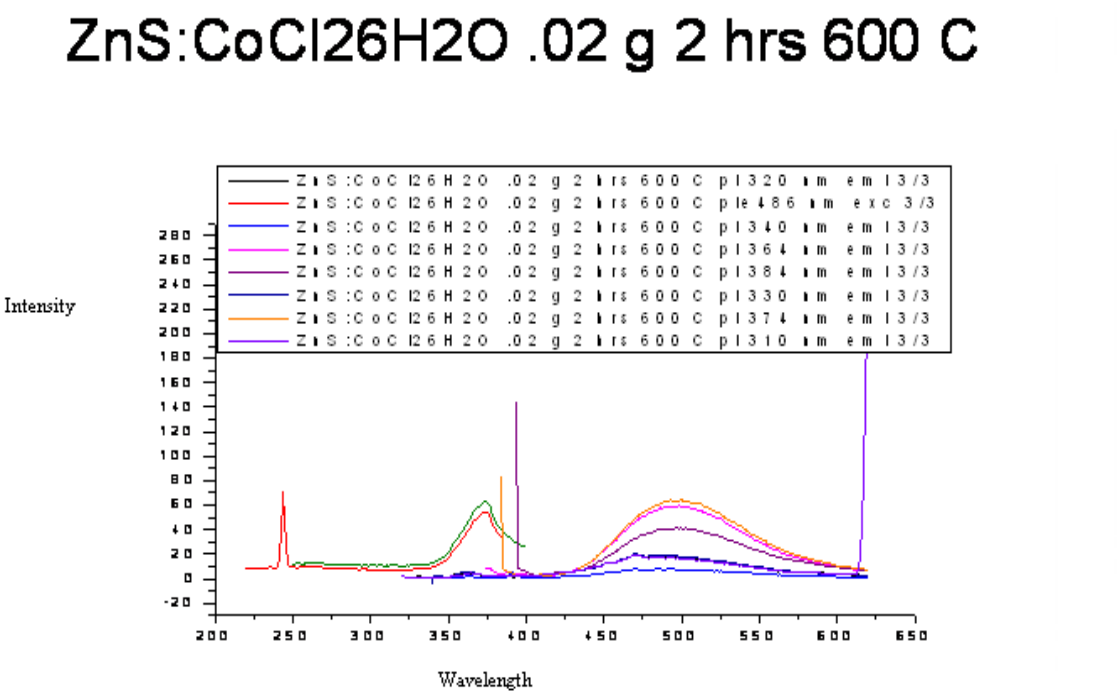

Fig. 3.3 PL Data of ZnS: $CoCl_2$ $6H_20$ .02 g 600 C showing both the excitation and emission spectra

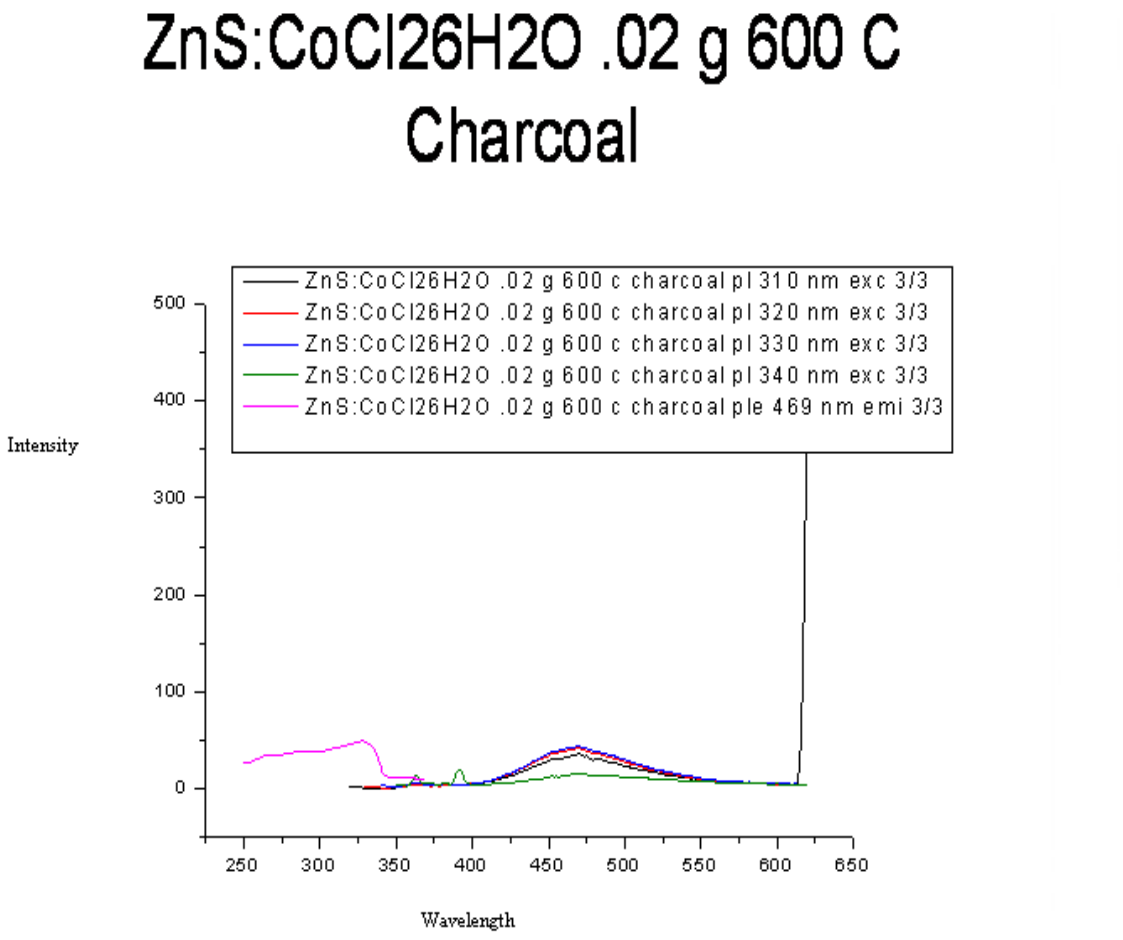

Fig. 3.4 PL Data of ZnS: $CoCl_2$ $6H_20$ .02 g 600 C Charcoal showing both the excitation and emission spectra

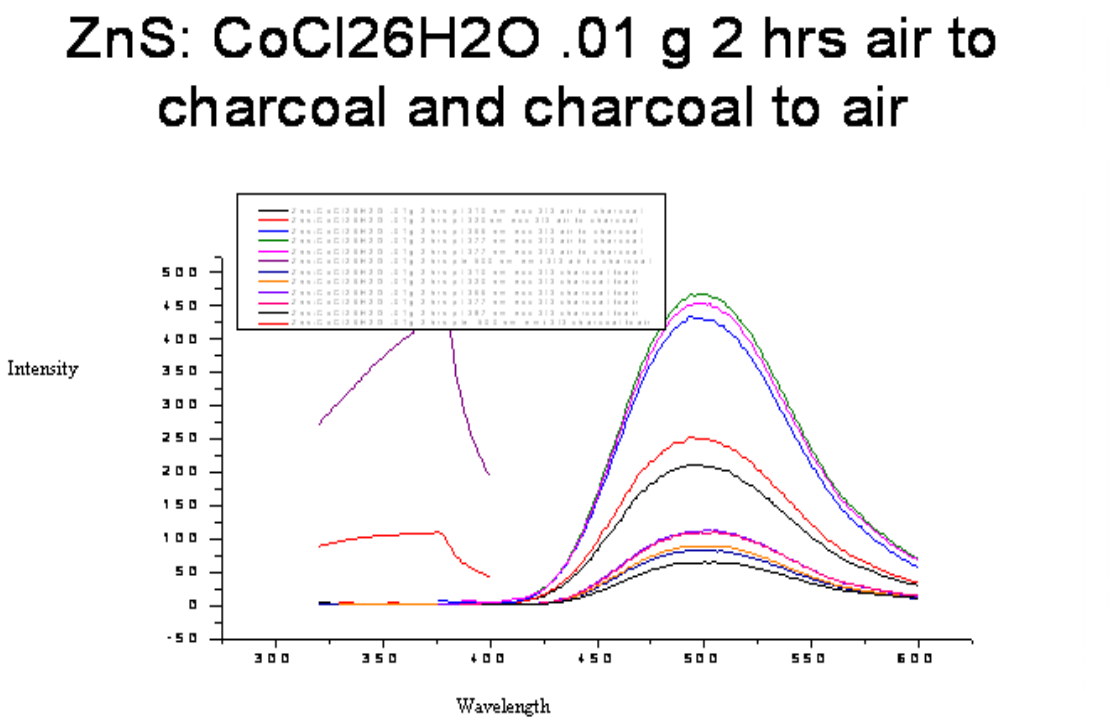

Fig. 3.5 PL Data of ZnS: $CoCl_2$ $6H_20$ .01 g 700 C Charcoal to air and air to charcoal showing both the excitation and emission spectra

By looking at the images of figures 3.1, 3.2, 3.3, 3.4, 3.5, one can see that the efficiency of the luminescence in ZnS will increase dramatically with the decrease in impurities which are given adding of the dopant ion of Co^{2+}. Another major difference is that the oxidation of ZnS provides the sample with a more intense emission spectrum in comparison to the samples which were covered by charcoal, which can be seen to have a poor effect on the intensity of the samples. The samples which were prepared under the condition of air to charcoal and the other sample which was made under charcoal and then moved to air saw no difference in the emission peaks; however, the intensity of the samples which were cooked under charcoal to air did see a greater jump in its intensity.

3.6 Tunneling Electron Microscope Data

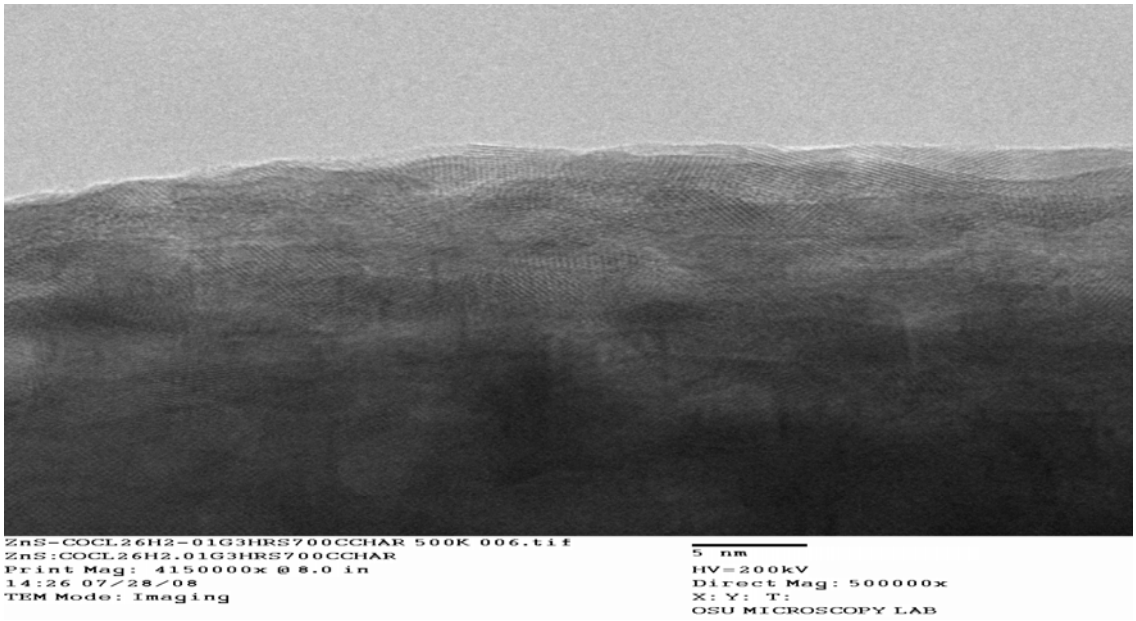

Fig. 3.6 TEM Data of lattice fringes of ZnS: CoCl26H2O .01g 3 hrs 700 C Charcoal

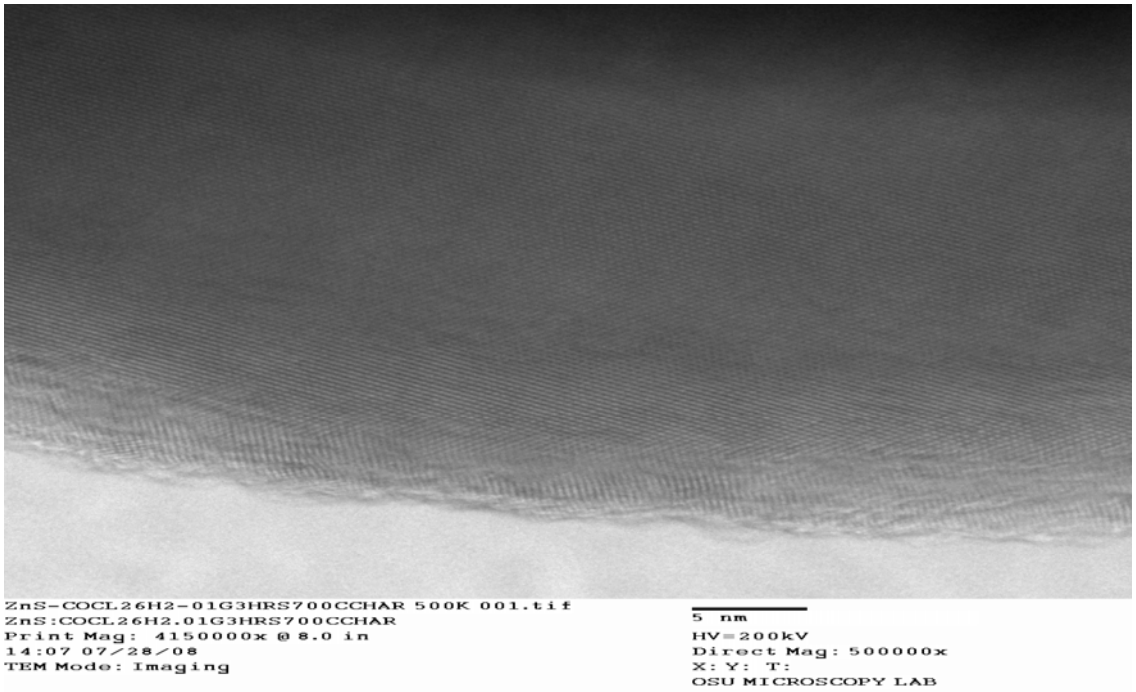

Fig. 3.7 TEM Data of lattice fringes of ZnS: CoCl26H2O .01g 3 hrs 700 C Charcoal

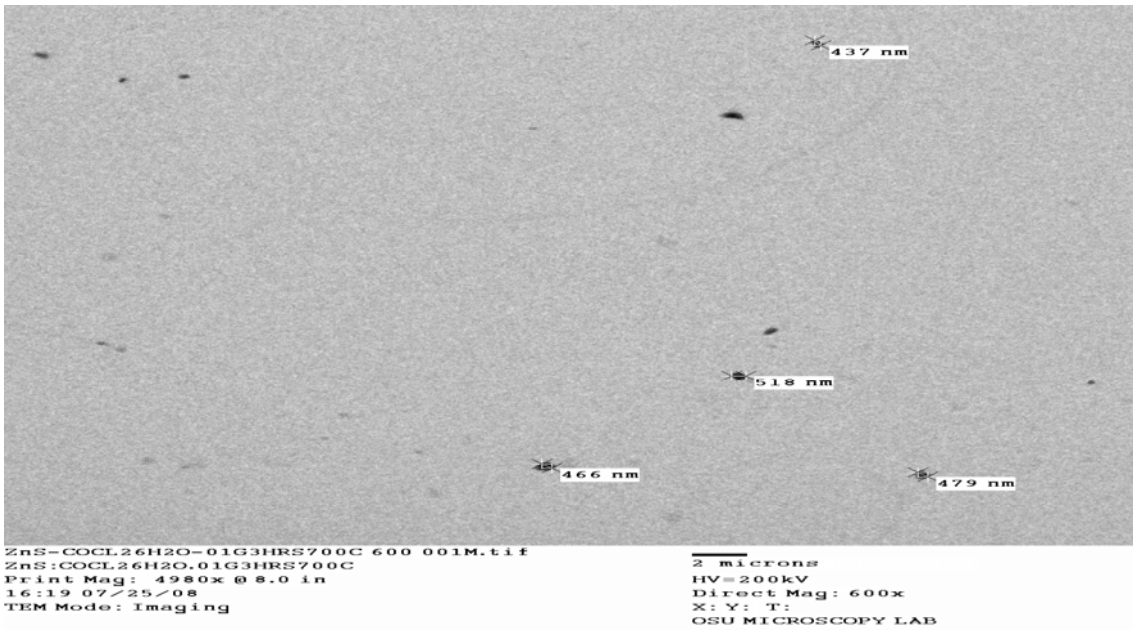

Fig. 3.8 TEM Data of ZnS: CoCl26H2O .01g 3 hrs 700 C showing scattered particles

From these images, the lattice constant was determined to be .48 nm from the sample of ZnS: $CoCl_2$ 6 H_2O under the charcoal which prevented the presence of oxygen to contaminate the sample during the cooking process. Futhermore, the average particle size from the image is found to be at 487 nm.

3.7 XRD Data for ZnS:Co2+

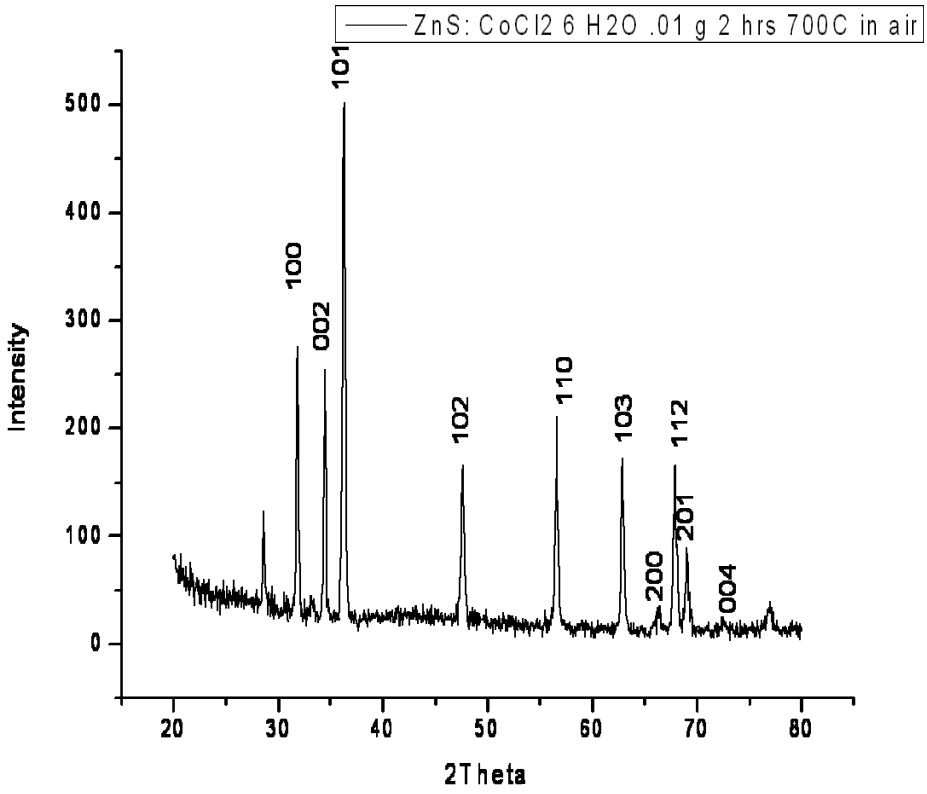

Fig. 3.9 XRD Measurements of ZnS: $CoCl_2$ $6H_2O$ .01 g 2 hrs 700 C in air showing characteristic peaks of a hexagonal form of ZnO

This diagram shows diffraction peaks at (100), (002), (101), (102), (110), (103), (200), (112) (201), (204) all correspond to characteristic peaks of zincite based on the reference of MDI Jade 5, which is a program used to analyze XRD data. Furthermore, the pdf reference is 36-1451, which shows that the pattern is that of hexagonal form of zinc oxide.

3.8 Photoluminescence Measurements of ZnS: AgCl

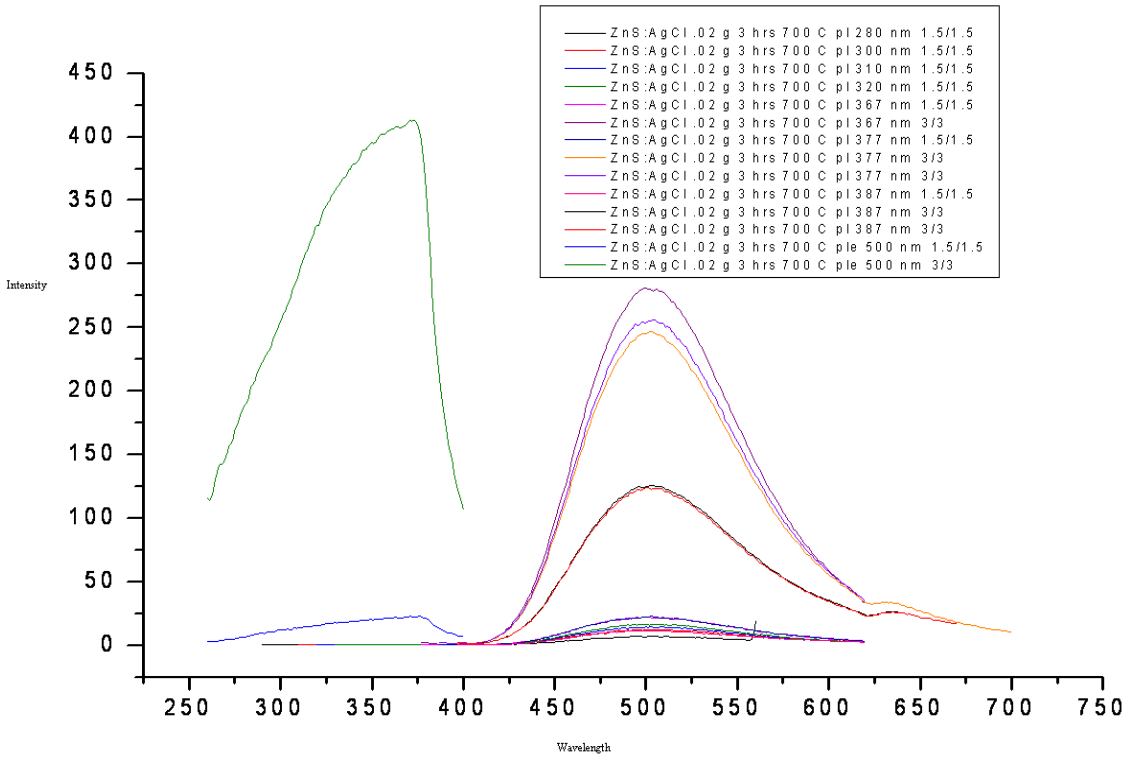

Fig. 3.10 PL Data of ZnS: AgCl .02g 3 hrs 700 C showing both the excitation and emission spectra

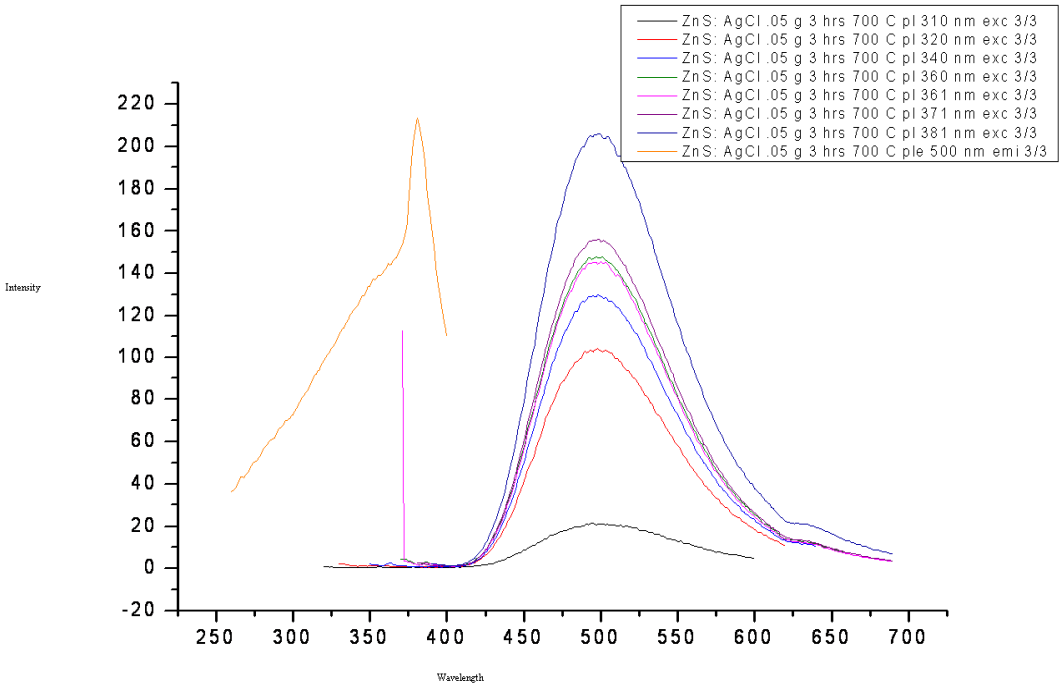

Fig. 3.11 PL Data of ZnS: AgCl .05 g 3 hrs 700C showing both the excitation and emission spectra

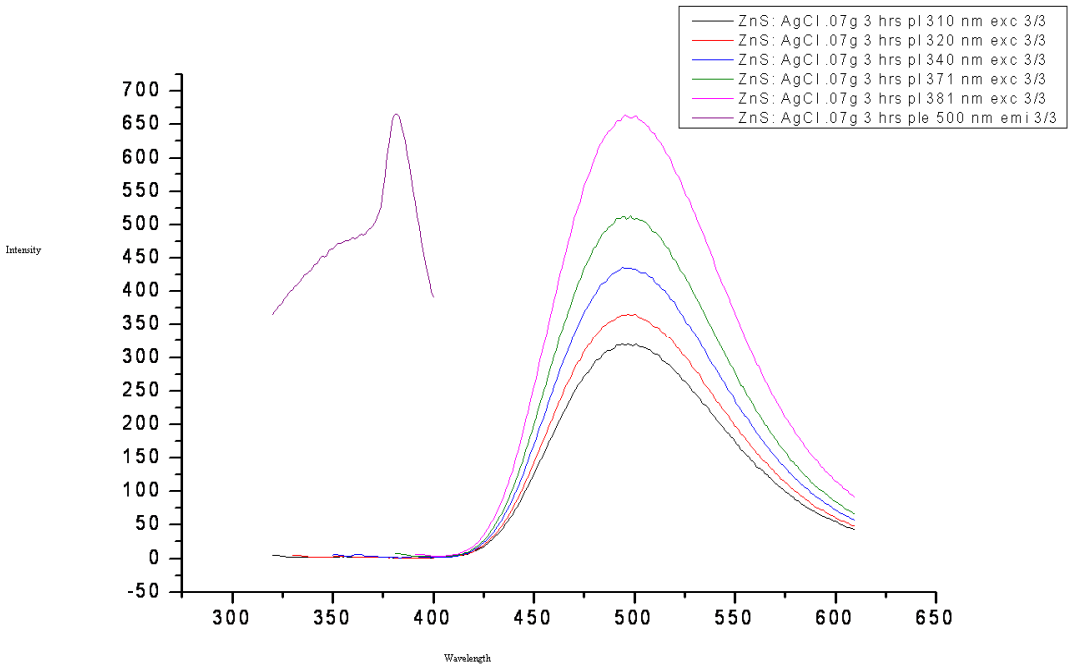

Fig. 3.12 PL Data of ZnS: AgCl .07 g 3 hrs 700C showing both the excitation and emission spectra

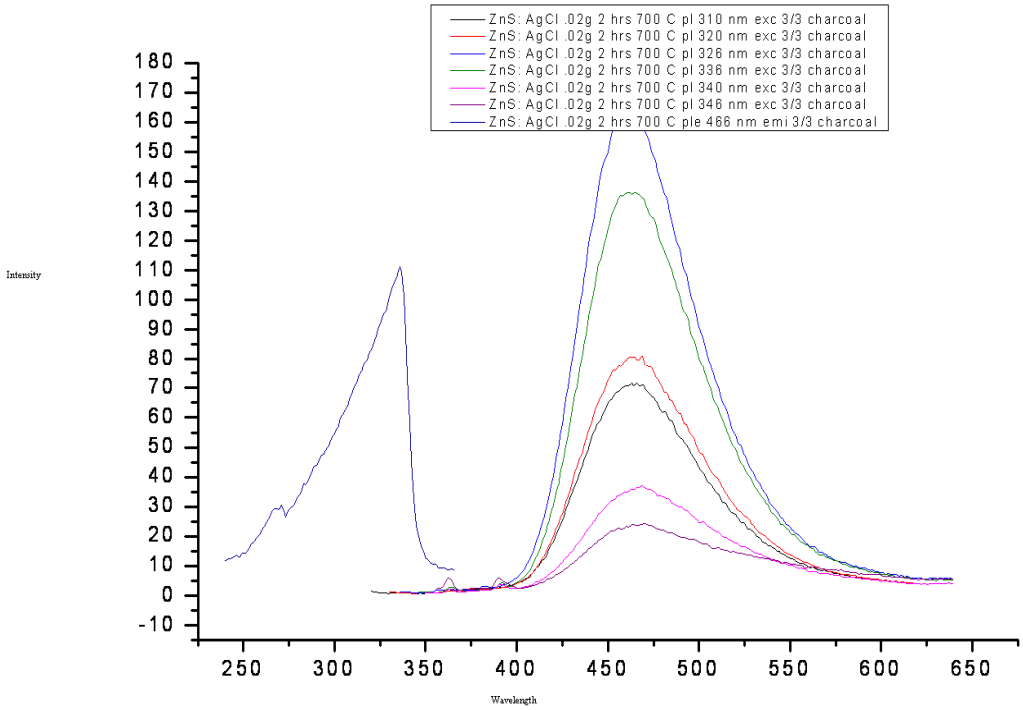

Fig. 3.13 PL Data of ZnS: AgCl .02 g 3 hrs 700C Charcoal showing both the excitation and emission spectra

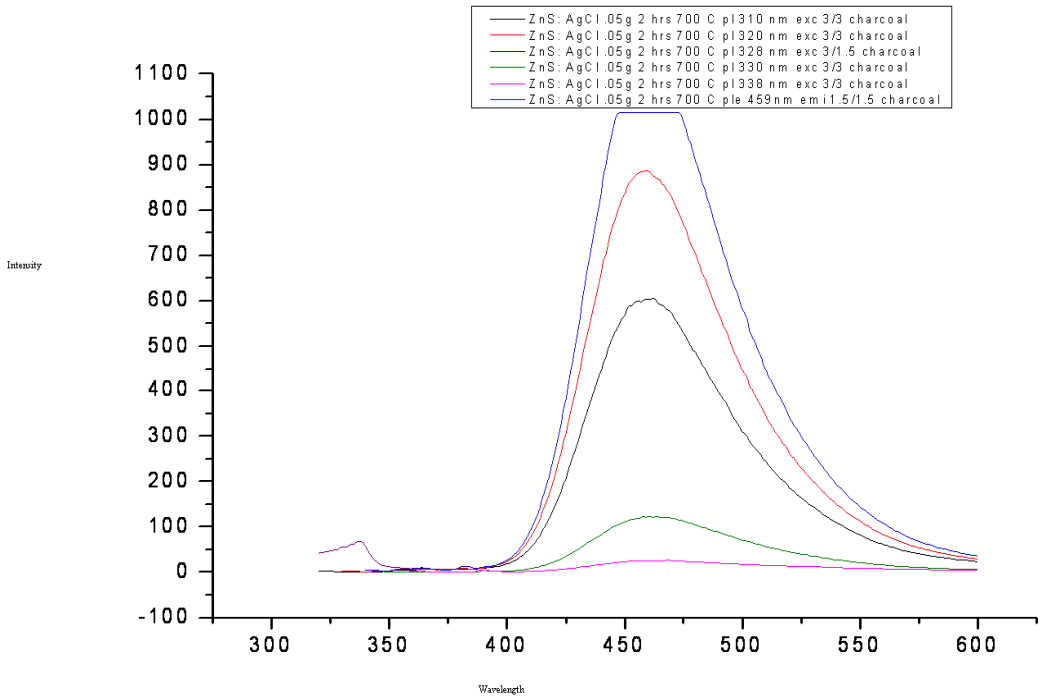

Fig. 3.14 PL Data of ZnS: AgCl .05 g 3 hrs 700C Charcoal showing both the excitation and emission spectra

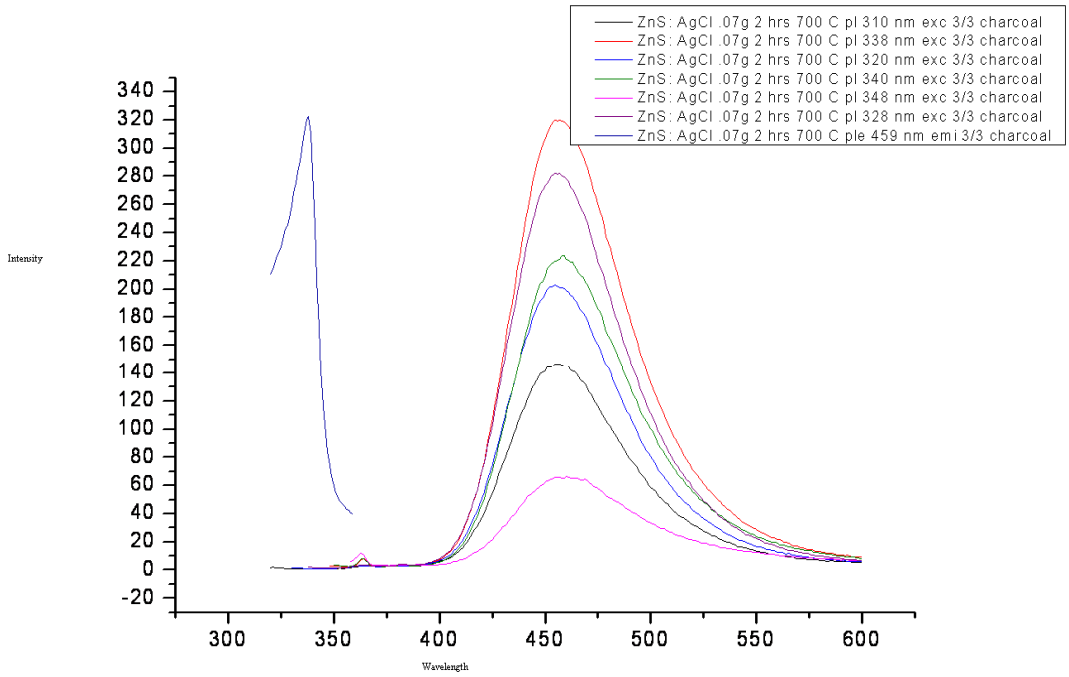

Fig. 3.15 PL Data of ZnS: AgCl .07 g 3 hrs 700C Charcoal showing both the excitation spectra and emission spectra

From the images, one can see how with the increase of dopant ions will increase the emission peak which is centered at 495 nm emission of the samples which are cooked in the atmosphere of air. Out of all the three samples, the sample which contains .07 g of Co2+ produces the most efficient and the most intense peak centered at 495 nm emission. The sample which is left in the atmosphere of air differs from the sample in charcoal due to dopant ion which is added and causes the emission peak to travel to the right of the spectrum, which is centered at 455 nm emission. Another major difference is the sample which contains .05 g of Ag^{1+}; it produces the most efficient and the most intense peak of all the three samples. Another observation was made

by switching samples which were made in air and under charcoal, respectively, and then switched to opposite conditions in order to observe what would happen. It was found that one can actually switch the emission peaks by changing the cooking conditions.

3.9 XRD Data for ZnS: Ag^{1+}

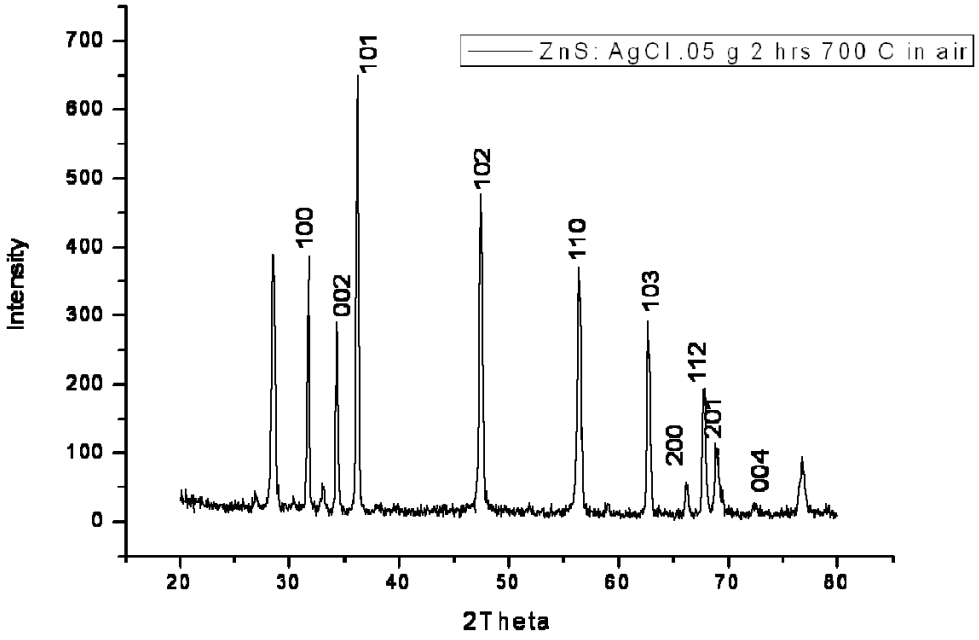

Fig. 3.16 XRD Data of ZnS: AgCl .05g 3 hrs 700 C showing characteristic peaks of ZnO

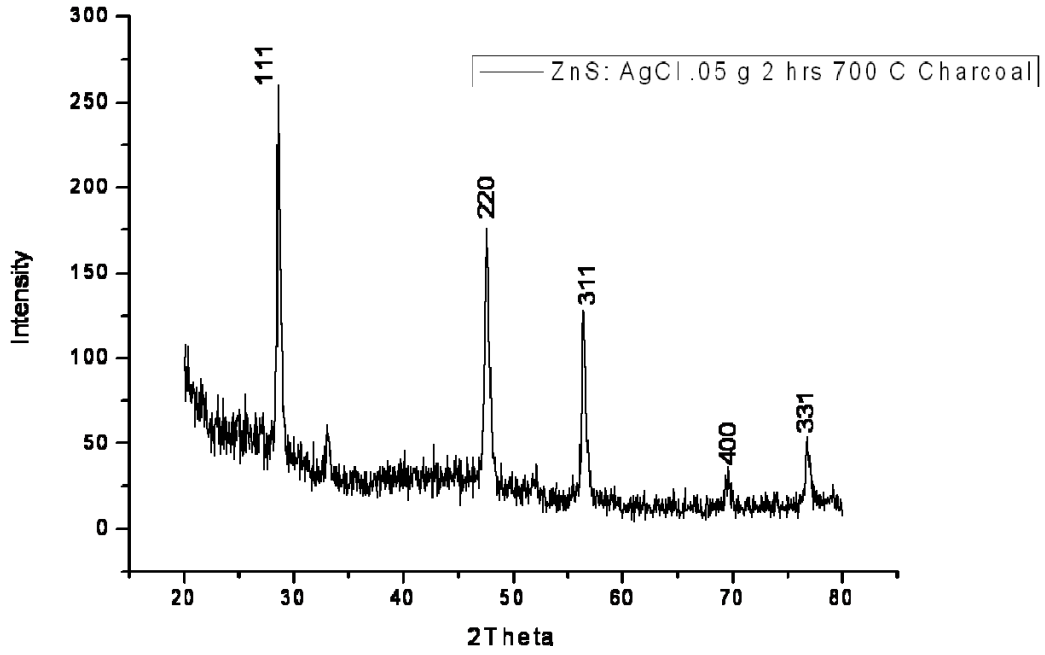

Fig. 3.17 XRD Data of ZnS: AgCl .05g 2 hrs 700 C Charcoal showing characteristic peaks of ZnS

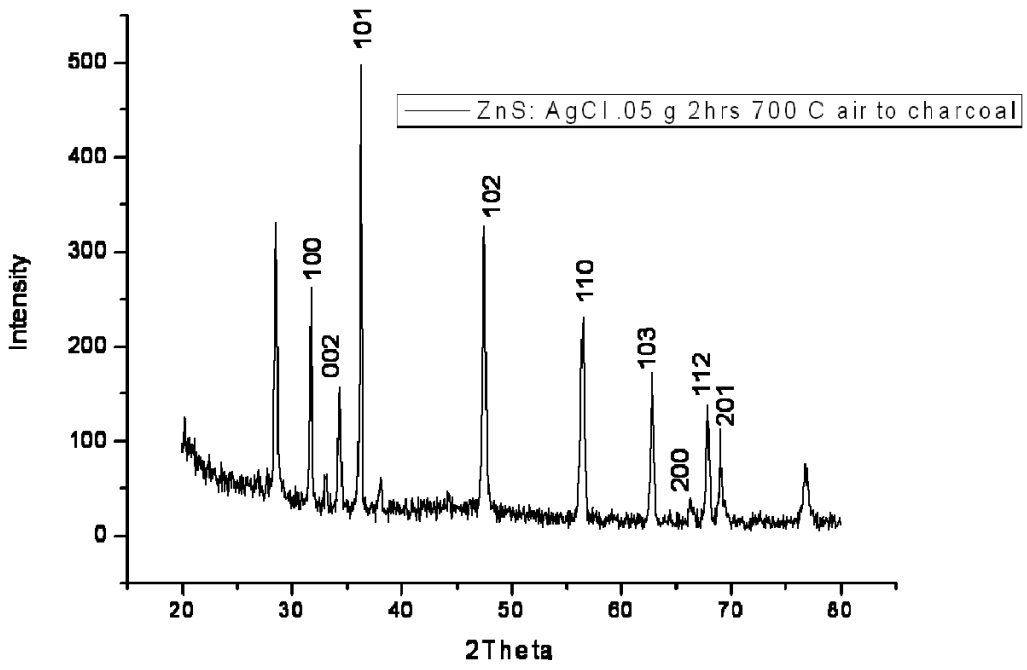

Fig. 3.18 XRD Data of ZnS: AgCl .05g 2 hrs 700 C Air to Charcoal showing characteristic peaks of ZnO

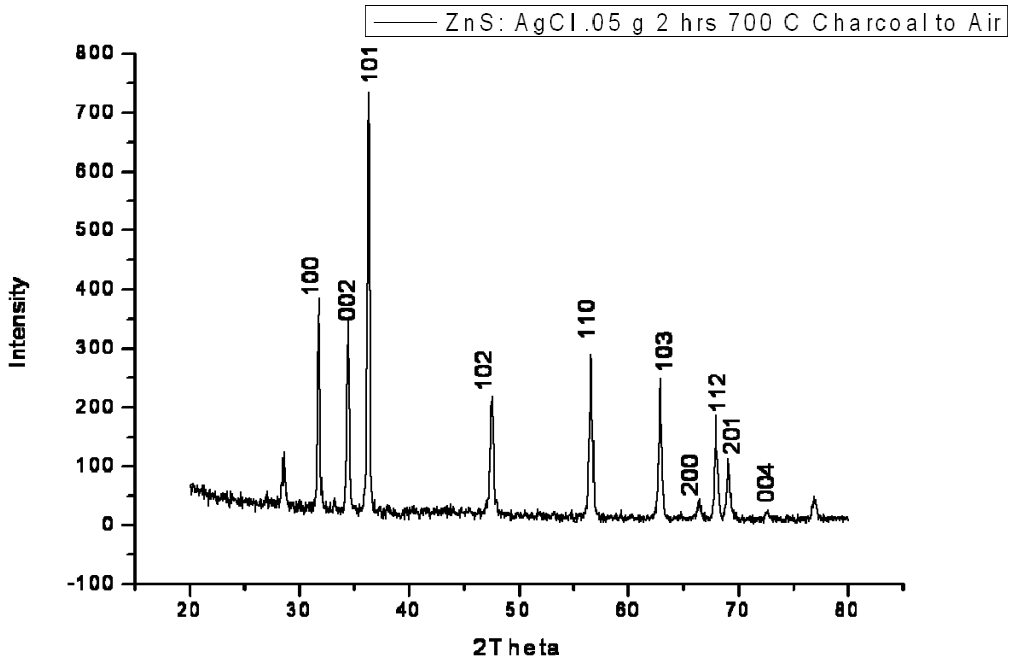

Fig. 3.19 XRD Data of ZnS: AgCl .05 g 2 hrs 700 C Charcoal to air showing characteristic peaks of ZnO

Figure 3.16, exhibits a cubic sphalerite form of ZnO based on the pdf 36-1451 with the use of MDI Jade, which was the software used to identify the following signature peaks. With the use of the Debye Scherrer formula this author was able to determine the average particle size to be 37.8 nm. Figure 3.17, is a sphalerite form of ZnS based on the pdf 05-0566 with the use of MDI Jade, which was the software used to identify the following signature peaks. With the use of the Debye Scherrer formula the particle size was determined to be 26.7 nm. From figure 3.18, one can see that the ZnO is a cubic sphalerite form based on the pdf 36-1451 with the use of MDI Jade, which was the software used to identify the following signature peaks. In figure 3.19, the ZnO is a cubic sphalerite form based on the pdf 36-1451 with the use of MDI Jade, which was the software used to identify the following signature peaks.

3.10 Conclusion

With the use of solid state diffusion, zinc sulfide can have its optical and structural properties by changing the amount of impurities which are added to the sample. To make a point, it was noticed that as Co^{2+} was added from .01g and .02g the intensity of the luminescence of the sample decreased, demonstrating that quenching occurred due to the increase of impurities. Moreover, in the samples of zinc sulfide which contained Ag^{1+}, the highest intensity occurred when .05 g were added and cooked under charcoal. The other sample which exhibited the highest intensity was the sample of zinc sulfide which had .07 g of silver chloride in it and was cooked under air. The structural properties of zinc sulfide doped with silver chloride were dependent on the cooking conditions of air and charcoal. The sample which was cooked under charcoal showed that no oxygen will contaminate the sample; therefore, the zinc sulfide remained. However, the sample of zinc sulfide cooked under air allowed for oxygen to enter, and after measuring the XRD peaks, it was found that zinc sulfide became zinc oxide. Consequently, cooking conditions affect the optical and structural properties of zinc sulfide.

CHAPTER 4

SUMMARY AND FUTURE WORK

With the emergence of flat emission display panels (FED's) and Plasma Display Panels (PDP's) the necessary materials to move this industry is the need for better luminescent materials. The material which has gained the attention from the scientific community has been Zinc Oxide which has intrinsic properties which can be used for many optoelectronic devices and for biological uses such as radiation detection.

In this work, ZnO: Eu^{3+} was synthesized using the method of solid state diffusion, where emissions can be tuned between green and red depending on the conditions of molar concentrations and temperature. With the production of these samples, measurements were taken to verify the structural and optical properties of the samples. Tunneling Electron Microscope Data was taken which showed the lattice constant to .50 which is slightly higher than the theoretical estimate of .45 nm. This can be attributed to the introduction of the dopant which stretched out the lattice structure. XPS data was taken which showed no difference in the chemical composition of the surface of the materials. The PL data showed for ZnO: Eu^{3+} .07 g cooked at 700 C for 2 hrs showed a green luminescence at 494 nm which is widely believed to be due to the strongly ionized oxygen vacancies. ZnO: Eu3+ .07 g cooked for 3 hrs at 600 C; ZnO: Eu3+ .16 g cooked for 2 hrs at 700 C; and ZnO: Eu^{3+} .16 g cooked for 2 hrs at 600 C, respectively, thus exhibiting a central luminescence peak centered around 615 nm which is done by lowest excited states [4] of Eu^{3+} $^5D_0$ to ^7F_J transitions. Based on the spectral analysis, it is concluded that there are three major peaks which correspond to the $^5D_0$ to ^7F_J these are seen at 590 nm, 610 nm and 625 nm, which are related to the $^5D_0$ to $^7F_1$, $^5D_0$ to $^7F_2$ and $^5D_0$ to $^7F_3$

transitions. [4] The largest emission peak is centered at 615 nm, which was caused by 467 nm excitation waveleng

From these studies, we can conclude that the optimal results for photoluminescence occurred between the temperatures of 600 C to 700 C which also showed as one increases the temperature of the cooking conditions it will also decrease the intensity of the luminescence. In addition, the different cooking conditions showed how ZnO: Eu^{3+} .07 g cooked for 2 hrs 700 C showed how Eu^{3+} won't be able to enter into the host lattice; however, the sample of ZnO: Eu^{3+} .07 g cooked for 2 hrs 600 C will be able to show the characteristic peaks of Eu^{3+}. The surface composition however revealed that Eu^{3+} for both the .07g sample cooked at 2 hrs for 700 C as well as the .16 sample cooked at 2 hrs 600 C showed Eu^{3+} was present in both samples at the surface of both samples. The TEM reveal that both the .07g sample cooked at 2 hrs for 700 C as well as the .16 sample cooked at 2 hrs 600 C show a crystalline structure was formed. However, the EDS data showed that no Eu^{3+} was present in the .07 g sample cooked for 2 hrs at 700 C.

Therefore, using solid state diffusion as method of synthesizing these samples we were able to use an efficient method of being able to engineer scintillators which can be manufactured to produce different emission wavelengths which can be used for radiation detection as well as other luminescent materials.

This investigation also showed the relationship between impurities and intensity of luminescence in ZnS: $CoCl_2$ $6H_2O$ and ZnS: AgCl. The samples which were cooked under charcoal and in the atmosphere of air showed two different emissions centered at 464 nm and 494 nm, respectively for both ZnS: Co^{2+} and ZnS: Ag^{1+}. The TEM data which was taken showed a lattice constant .48 nm under charcoal which prevented oxygen to contaminate the samples. The XRD data showed characteristic peaks for ZnS cooked under air and ZnO cooked under charcoal. Therefore, oxidation changes not only the structural components of but also the luminescent properties of the sample itself.

More work must be done to understand how these samples will react under ionizing radiation and how this can be used to better radiation detection for biological applications as well as homeland security applications.

REFERENCES

[1] Y.K. Park, J.I. Han, M.G. Kwak et al 1997 Appl. Phys. Lett. 72 668-670

[2} S.A.M. Lima, F.A. Sigoli, M.R. Davalos, M. Jafelicci Jr. 2002 Journal of Alloys and Compounds 344 280-284

[3] Hayashi Y et al 1995 Jpn. J. Appl. Phys. 34 1878

[4] Mingya Zhong, Guiye Shan, Yajan Li et al 2007 Material Chemistry and Physics 106 305-309

[5] Kouyate D et al 1991 J. Lumin. 50 205

[6] S.E. Dorenzo, M.J. Weber, E. Bourret-Courchesne, M.K. Klintenberg 2003 Nuclear and Instruments and Methods in Physics Research 505 111-117

[7] Weber, M. J. 2004 Nuclear Instruments and Methods in Physics Research 527 9-14

[8] P. Lecoq, A. Annenkov. A. Gektin, M. Korzhik, C. Pedrini Inorganic Scintillators for Detector Systems: Physical Properties and Crystal Engineering 2006 Springer

[9} Yen, William M. and Weber, Marvin J. Inorganic Phosphors-Compositions, Preparation and Optical Properties 2004 CRC Press

[10] Look, David C. Zinc Oxide Bulk, Thin Films, and Nanopowders 2006 Elsevier

[11] Ü. Özgür and H. Morkoç Zinc Oxide Bulk, Thin Films, and Nanopowders 2006 Elsevier

[12] Zhang, Lin li, Guo, Chang, Xin, Zhao, Jun Jin et al 2005 Chin. Phys. Lett. Vol 22, No. 5 1225

[13] P. Yang, M. Lü, D. Xü, D. Yuan, C. Song, G. Zhou 2001 Journal of Physics and Chemistry of Solids 62 1181-11184

[14] P. Yang, M. Lü, G. Zhou, D. Yuan, D. Xü 2001 Inorganic Chemistry Communications 4 737-737

[15] G. Blasse, B.C. Grabmaier Luminescent Materials 1194 Spinger Verlag

BIOGRAPHICAL INFORMATION

The author received his Bachelor of Science degree in physics from the University of Texas at Arlington in May 2005. He received a Master of Science degree in degree from the University of Texas in December 2008. He will continue studying for his Ph.D